





# Extension of O-Linked Mannosylation in the Golgi Apparatus Is Critical for Cell Wall Integrity Signaling and Interaction with Host Cells in *Cryptococcus neoformans* Pathogenesis

Eun Jung Thak,<sup>a</sup> Ye Ji Son,<sup>a</sup> Dong-Jik Lee,<sup>a</sup> Hyunah Kim,<sup>a</sup> Jung Ho Kim,<sup>a</sup> Su-Bin Lee,<sup>a</sup> Yu-Byeong Jang,<sup>b</sup>  Yong-Sun Bahn,<sup>b</sup> Connie B. Nichols,<sup>c</sup>  J. Andrew Alspaugh,<sup>c</sup>  Hyun Ah Kang<sup>a</sup>

<sup>a</sup>Department of Life Science, Chung-Ang University, Seoul, Republic of Korea

<sup>b</sup>Department of Biotechnology, College of Life Science of Biotechnology, Yonsei University, Seoul, Republic of Korea

<sup>c</sup>Department of Medicine, Duke University School of Medicine, Durham, North Carolina, USA

Eun Jung Thak and Ye Ji Son contributed equally to this work. Author order was determined in order of increasing seniority.

**ABSTRACT** The human-pathogenic yeast *Cryptococcus neoformans* assembles two types of O-linked glycans on its proteins. In this study, we identified and functionally characterized the *C. neoformans* *CAP6* gene, encoding an  $\alpha$ 1,3-mannosyltransferase responsible for the second mannose addition to minor O-glycans containing xylose in the Golgi apparatus. Two cell surface sensor proteins, Wml1 (*WSC/Mid2-like*) and Wml2, were found to be independent substrates of Cap6-mediated minor or Ktr3-mediated major O-mannosylation, respectively. The double deletion of *KTR3* and *CAP6* (*ktr3Δ cap6Δ*) completely blocked the mannose addition at the second position of O-glycans, resulting in the accumulation of proteins with O-glycans carrying only a single mannose. Tunicamycin (TM)-induced phosphorylation of the Mpk1 mitogen-activated protein kinase (MAPK) was greatly decreased in both *ktr3Δ cap6Δ* and *wml1Δ wml2Δ* strains. Transcriptome profiling of the *ktr3Δ cap6Δ* strain upon TM treatment revealed decreased expression of genes involved in the Mpk1-dependent cell wall integrity (CWI) pathway. Consistent with its defective growth under several stress conditions, the *ktr3Δ cap6Δ* strain was avirulent in a mouse model of cryptococcosis. Associated with this virulence defect, the *ktr3Δ cap6Δ* strain showed decreased adhesion to lung epithelial cells, decreased proliferation within macrophages, and reduced transcytosis of the blood-brain barrier (BBB). Notably, the *ktr3Δ cap6Δ* strain showed reduced induction of the host immune response and defective trafficking of ergosterol, an immunoreactive fungal molecule. In conclusion, O-glycan extension in the Golgi apparatus plays critical roles in various pathobiological processes, such as CWI signaling and stress resistance and interaction with host cells in *C. neoformans*.

**IMPORTANCE** *Cryptococcus neoformans* assembles two types of O-linked glycans on its surface proteins, the more abundant major O-glycans that do not contain xylose residues and minor O-glycans containing xylose. Here, we demonstrate the role of the Cap6  $\alpha$ 1,3-mannosyltransferase in the synthesis of minor O-glycans. Previously proposed to be involved in capsule biosynthesis, Cap6 works with the related Ktr3  $\alpha$ 1,2-mannosyltransferase to synthesize O-glycans on their target proteins. We also identified two novel *C. neoformans* stress sensors that require Ktr3- and Cap6-mediated posttranslational modification for full function. Accordingly, the *ktr3Δ cap6Δ* double O-glycan mutant strain displays defects in stress signaling pathways, CWI, and ergosterol trafficking. Furthermore, the *ktr3Δ cap6Δ* strain is completely avirulent in a mouse infection model. Together, these results demonstrate critical roles for O-glycosylation in fungal pathogenesis. As there are no human homologs for Cap6 or Ktr3, these fungus-specific mannosyltransferases are novel targets for antifungal therapy.

**Editor** Michael Lorenz, University of Texas Health Science Center

**Copyright** © 2022 Thak et al. This is an open-access article distributed under the terms of the [Creative Commons Attribution 4.0 International license](https://creativecommons.org/licenses/by/4.0/).

Address correspondence to J. Andrew Alspaugh, [andrew.alspaugh@duke.edu](mailto:andrew.alspaugh@duke.edu), or Hyun Ah Kang, [hyunkang@cau.ac.kr](mailto:hyunkang@cau.ac.kr).

The authors declare no conflict of interest.

**Received** 2 August 2022

**Accepted** 27 October 2022

**KEYWORDS** *Cryptococcus neoformans*, protein O-mannosylation, *KTR3*, *CAP6*, fungal pathogenesis

Protein O-mannosylation, a type of posttranslational modification, is evolutionarily conserved from bacteria to humans with structural variation (1, 2). Protein O-mannosyltransferases (PMTs) initiate O-mannosylation in the endoplasmic reticulum (ER) by transferring mannose to serine or threonine residues of target proteins, a highly conserved aspect of protein glycosylation in eukaryotes (3, 4). However, the processing of O-mannosylation in the Golgi apparatus shows several species-specific features. In yeast and filamentous fungi, the  $\alpha$ 1,2-linked mannotriose (Man $\alpha$ 1-2Man $\alpha$ 1-2Man $\alpha$ 1-Ser/Thr) is the most common core form, which is further extended in the Golgi apparatus by specific mannosyltransferases, generating short oligomannose chains with diverse structures depending on the species (5–8). In mammals, a variety of monosaccharides besides mannose can be O-linked to proteins, such as N-acetylgalactosamine, galactose, or glucose, followed by the addition of other sugars (9).

Protein O-mannosylation has critical biological roles, including directing cell morphology, protein stability, protein secretion, protein degradation, and cell wall integrity (CWI), in yeast and filamentous fungi (10–12). Involvement of O-mannosylation in virulence and development has been also reported for several fungal pathogens (13). In the human-pathogenic fungus *Candida albicans*, Pmt4-mediated O-mannosylation has roles in environment-specific morphogenetic signaling and full virulence (14). The disruption of *C. albicans* *MNT1* and *MNT2*, encoding partially redundant  $\alpha$ -1,2-mannosyltransferases that catalyze the addition of the second and third mannose residues of O-glycans in the Golgi apparatus, results in altered cell morphology, hypersensitivity to cell wall-perturbing agents, and attenuated virulence in a murine model of systemic infection (15). In *Aspergillus fumigatus*, the *MNT1* deletion mutant strain shows reduced cell wall thickness, cell growth, conidium formation, and attenuated virulence (16). In the dimorphic fungal pathogen *Histoplasma capsulatum*, the *pmt1* $\Delta$  and *pmt2* $\Delta$  null mutants exhibit attenuated virulence because protein O-mannosylation is required for its thermotolerance at mammalian body temperature (17). Pleiotropic roles for the O-mannosyltransferase MoPmt4 were recently reported in the development and pathogenicity of the plant pathogen *Magnaporthe oryzae* (18). Additionally, *pmt* $\Delta$  mutants display impaired growth, reduced conidiation, defective cell walls, enhanced endoplasmic reticulum (ER) stress, and attenuated virulence in *Fusarium oxysporum* f. sp. *cucumerinum* (19).

Glycoproteins on the cell surface of fungal pathogens could contribute to interaction with host cells, and these interactions might be affected by altered glycan structures (20). In *C. albicans*, *pmt1* $\Delta$  and *mnt1* $\Delta$  *mnt2* $\Delta$  mutants are defective in their ability to induce host proinflammatory cytokines such as granulocyte colony-stimulating factor (G-CSF), granulocyte-macrophage colony-stimulating factor (GM-CSF), and interleukin 6 (IL-6). Moreover, these mutants show reduced ability to damage oral epithelial cells (21). Cell wall remodeling resulting in exposed glycosylated proteins is required for *C. albicans*-induced pyroptosis, a form of necrotic cell death mediated by inflammasomes (22, 23). Interestingly, O-mannosylated proteins, such as mannoprotein Dan1 acting as an ergosterol receptor, have been proposed to affect pyroptosis by altering ergosterol localization. Pmt4-mediated O-mannosylation has been shown to be especially required for *C. albicans*-induced pyroptosis (24).

*Cryptococcus neoformans* is an opportunistic fungal pathogen that causes life-threatening meningoencephalitis in immunocompromised hosts after crossing the blood-brain barrier (BBB). In pathogenic *Cryptococcus* species, several extracellular factors contribute to virulence, including the polysaccharide capsule, melanin pigment, and various hydrolytic enzymes (25). In addition, many secreted mannoproteins are key factors of *C. neoformans* pathogenicity (26, 27) and evoke specific immune responses (28). In *C. neoformans*, the PMT family, composed of three members, Pmt1, Pmt2, and Pmt4, was previously reported to initiate protein O-mannosylation. *PMT2* is an essential gene, and the *pmt1* $\Delta$

and *pmt4* $\Delta$  mutants show attenuated virulence in a murine inhalation model of cryptococcosis (10, 29). The presence of a xylose-phosphate-mannose linkage, mediated by Xpt1, was reported in *C. neoformans* O-linked glycans (30). Subsequently, systematic analysis of the O-glycan structure indicated that *C. neoformans* has two O-mannosylation pathways, a major pathway generating short mannosylated glycans without xylose modification (Man<sub>1</sub>-Man<sub>4</sub>) and a minor pathway with xylose addition (Xyl<sub>1</sub>Man<sub>2</sub>-Xyl<sub>1</sub>Man<sub>4</sub>) (31).

In this study, we report that *C. neoformans* Cap6 is responsible for the second mannose addition in  $\alpha$ 1,3-linkage to the minor O-glycans in the Golgi apparatus. Notably, two novel cell surface sensor proteins, Wml1 and Wml2, are identified as independent substrates of Cap6-mediated minor and Ktr3-mediated major O-mannosylation, respectively. By systematic analysis of the *ktr3* $\Delta$  *cap6* $\Delta$  double mutant, we demonstrate the critical roles of the O-glycan extension in activating CWI signaling pathways and in mediating host cell interaction during sequential steps of the infection process. We further present data supporting the requirement of O-glycan extension for the host immune response, partly by involvement in ergosterol trafficking.

## RESULTS

**Cap6 adds the second mannose residue for xylose addition in minor O-linked glycans.** *Cryptococcus neoformans* has two O-mannosylation pathways, the major pathway that mediates O-mannosyl additions that do not contain xylose and the minor pathway that mediates additions containing xylose (31). Ktr3 ( $\alpha$ 1,2-mannosyltransferase) is responsible for the addition of the second mannose residue in the major O-glycan synthesis pathway. However, the presence of xylose-containing O-glycans in the *ktr3* $\Delta$  mutant implies that extension of minor O-glycans in *C. neoformans* occurs by the action of another specific mannosyltransferase, independent of Ktr3. We hypothesized that the mannose residue at the second position of minor O-glycans, at which xylose is attached (31), should have an  $\alpha$ 1,3-linkage considering that a xylose residue is attached to the mannose backbone that has  $\alpha$ 1,3-linkage in *C. neoformans* capsules (32, 33) and N-glycans (34). To confirm this possibility, we collected and analyzed the M2 peak from the *C. neoformans* *ktr3* $\Delta$  strain (see Fig. S1A in the supplemental material). Comparison of the high-performance liquid chromatography (HPLC) elution profile with standard  $\alpha$ 1,2-mannobiose and  $\alpha$ 1,3-mannobiose indicated that the second mannose residue of *C. neoformans* minor O-glycans is added in an  $\alpha$ 1,3-linkage to the first mannose residue (Fig. S1A), in contrast to the  $\alpha$ 1,2-linkage of the second mannose residue in major O-glycans. To define the  $\alpha$ 1,3-mannosyltransferase that adds the second mannose residue to minor O-glycans in *C. neoformans*, we selected two proteins, Cap6 (CNAG\_06016) and Cmt1 (CNAG\_03158), which were previously identified based on their homology to Cap59, an  $\alpha$ 1,3-mannosyltransferase involved in capsule synthesis (35, 36). Multiple sequence alignment of Cap59 homologs revealed that *C. neoformans* Cap59, Cap6, and Cmt1 have a DXD (aspartate-any residue-aspartate) motif, essential for enzymatic activity and commonly found in glycosyltransferases (Fig. S1B). Cmt1 was suggested to be involved in the synthesis of the capsule polymer glucuronoxylomannan (GXM), but deletion of *CMT1* does not affect capsule formation (35). Cap6 is homologous to both Cmt1 and Cap59 (36). However, a previous deletion study similarly reported that Cap6 is not involved in capsule formation (37), leaving open questions on the physiological role of Cap6.

We disrupted the *CMT1* and *CAP6* genes (Fig. S2A) and analyzed the O-glycan profiles of the *cmt1* $\Delta$  and *cap6* $\Delta$  strains. Although no apparent differences were observed in the O-glycan profile of the *cmt1* $\Delta$  mutant compared with that of the wild-type (WT) strain (data not shown), the *cap6* $\Delta$  mutant showed reduced peaks corresponding to the minor X1M2 to X1M4 oligosaccharides by HPLC analysis. Reintroduction of the WT *CAP6* gene into the *cap6* $\Delta$  mutant restored the X1M2 to X1M4 peaks (Fig. 1A). The O-glycan profile of the *ktr3* $\Delta$  *cap6* $\Delta$  double mutant strain displayed only the M1 peak, in which the first mannose residue is added to serine or threonine of proteins by *PMT* gene families in the ER (Fig. 1A). Reintroduction of *CAP6* and *KTR3* into the *ktr3* $\Delta$  *cap6* $\Delta$  mutant (*ktr3* $\Delta$  *cap6* $\Delta$ ::*CAP6* strain and *ktr3* $\Delta$  *cap6* $\Delta$ ::*KTR3* strain) (Fig. S2B and C)

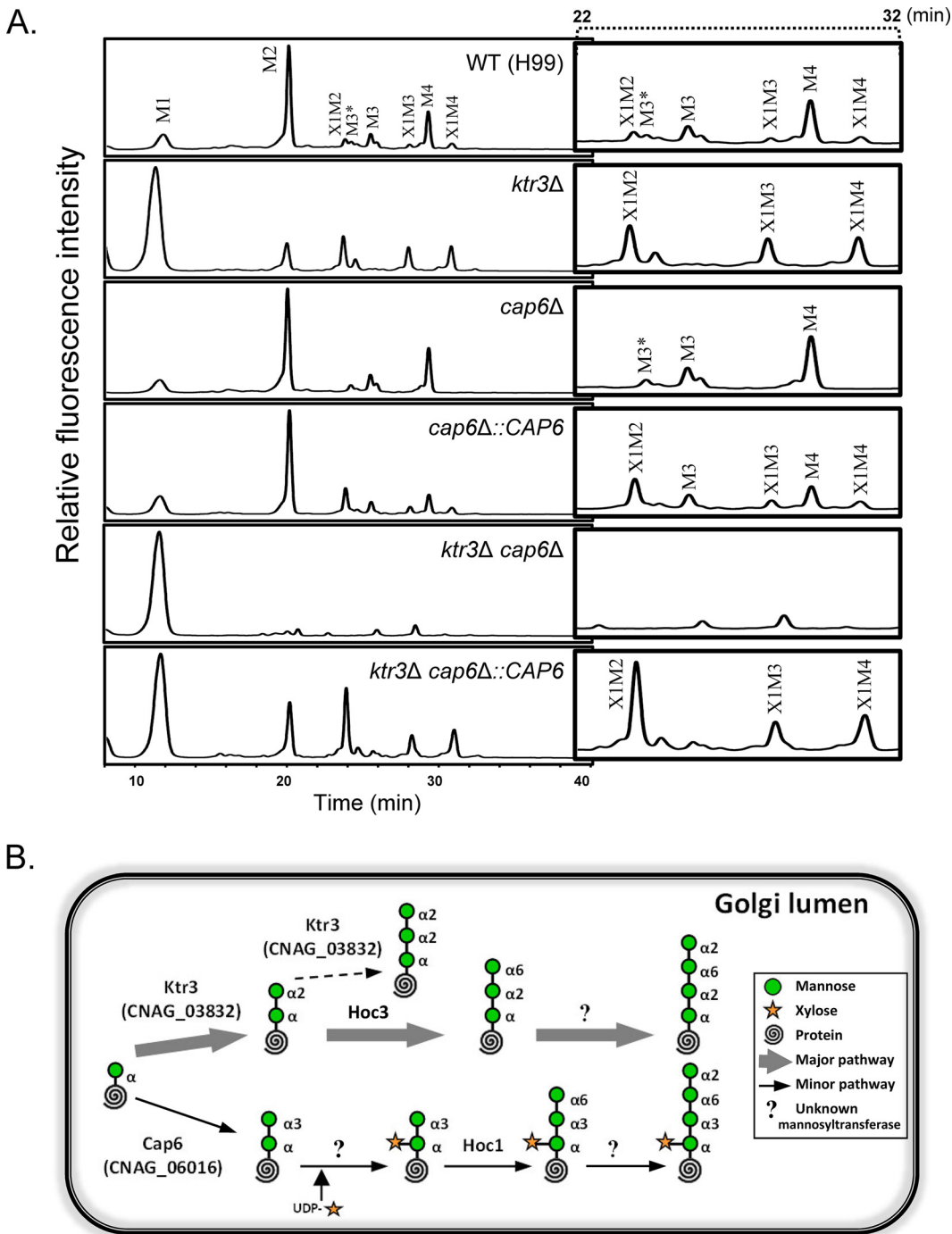


**FIG 1** Functional analysis of Cap6 as  $\alpha$ 1,3-linked mannosyltransferase responsible for biosynthesis of minor O-linked glycans. (A) HPLC profiles of O-glycans of cell wall mannoproteins (cwMPs) from WT, *ktr3* $\Delta$ , *cap6* $\Delta$ , *cap6* $\Delta$ ::CAP6, *ktr3* $\Delta$  *cap6* $\Delta$ , and *ktr3* $\Delta$  *cap6* $\Delta$ ::CAP6 strains. To distinguish small peaks more clearly, the HPLC profiles from 22 to 32 min in the x and y axes were enlarged and inserted. M, mannose; X, xylose; M3\*,  $\alpha$ 1,2-mannotriose. (B) Schematic representation of the proposed O-glycosylation pathway in *C. neoformans* assigned with Cap6.

restored the altered O-glycan profile to the almost identical profiles of the *ktr3* $\Delta$  and *cap6* $\Delta$  strains, respectively (Fig. 1A; Fig. S2D). These results demonstrate that Cap6 is responsible for the addition of the second  $\alpha$ 1,3-mannose residue in the biosynthetic pathway of minor O-glycans (Fig. 1B). This also strongly supports that the  $\alpha$ 1,3-linkage is an important determinant for xylose addition not only in capsules but also in glycans assembled on proteins.

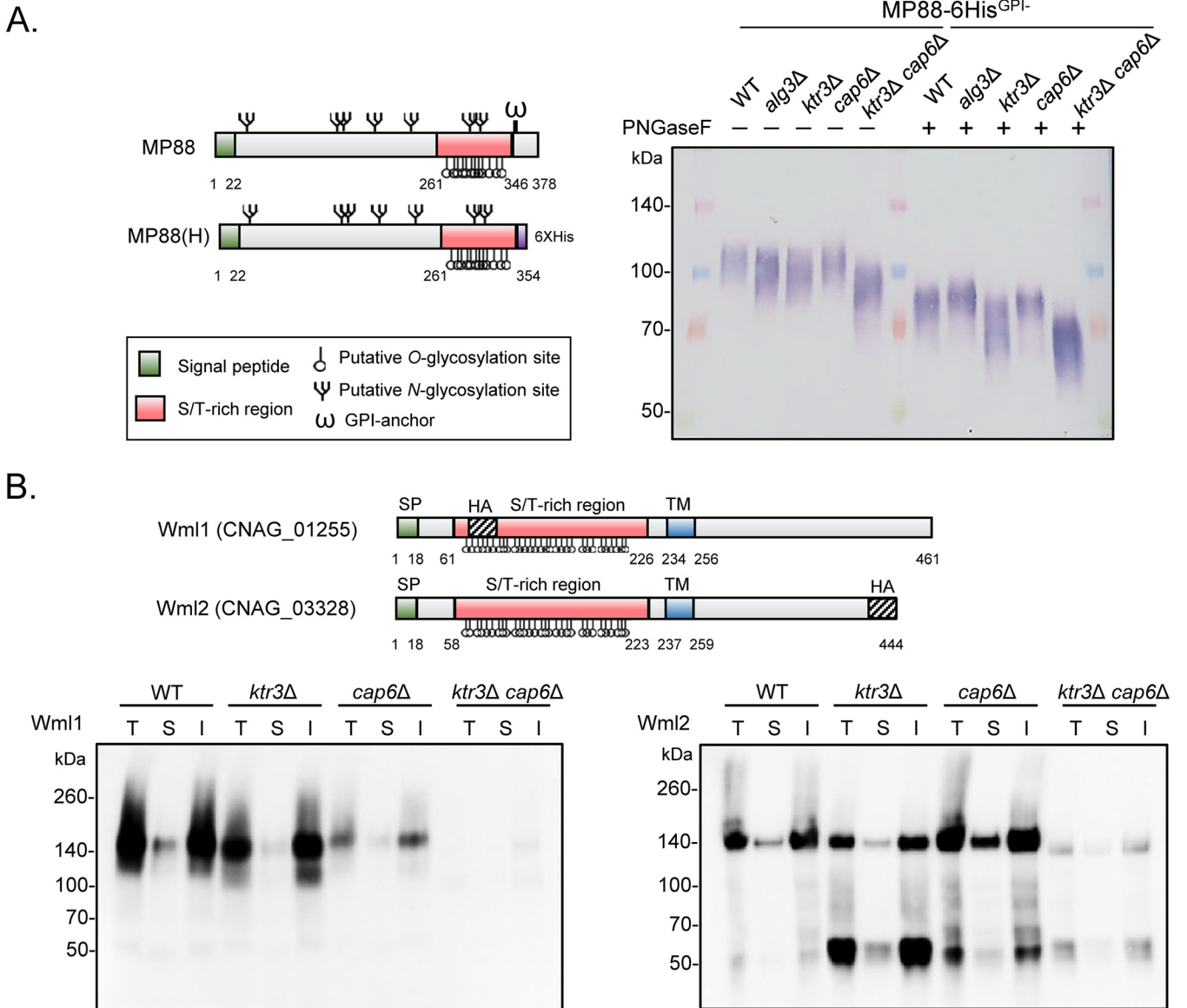


**FIG 2** Glycosylation pattern analysis of *C. neoformans* O-glycan mutant strains. (A) Western blot of MP88 protein secreted from several *N*- or O-glycosylation mutants of *C. neoformans*, including *alg3Δ*, *ktr3Δ*, *cap6Δ*, and *ktr3Δ cap6Δ* mutants. Yeast cells were cultivated in YPD medium for 24 h and harvested, and the culture supernatants were TCA precipitated and subjected to Western blot analysis with anti-His antibody. (B) Western blot analysis of Wml1 and Wml2 in *C. neoformans* O-glycan-deficient mutant strains. Domain structure of putative cell wall stress sensors, Wml1 and Wml2. Circle symbol indicates O-glycosylation sites, predicted by YinOYang1.2. Subcellular fractionation was subjected to Western blot analysis with anti-HA antibody, as described in Text S1 in the supplemental material. T, total; S, soluble; I, insoluble; TM, transmembrane domain.

**Ktr3 and Cap6 function independently in O-linked protein mannosylation of *C. neoformans*.** To investigate the effect of *KTR3* and *CAP6* deletions on protein O-mannosylation, we examined the glycosylation pattern of mannoprotein 88 (MP88), which was reported to stimulate T-cell responses and to be involved in the *C. neoformans*-epithelial lung cell adhesion (38). MP88 is predicted to contain 7 *N*-glycosylation sites and 41 O-glycosylation sites. To analyze the glycosylation patterns of MP88, His-tagged and glycosylphosphatidylinositol (GPI)-anchorless MP88 was expressed in various glycosylation mutant strains, including *alg3Δ*, *ktr3Δ*, *cap6Δ*, and *ktr3Δ cap6Δ* strains (Fig. 2A). The migration of MP88 protein was altered in the *alg3Δ* mutant, which has a defect in the biosynthesis of core *N*-linked glycans (39), indicating that MP88 protein is subjected to *N*-glycosylation. The MP88 protein did not show a detectable change in apparent molecular weight (MW) in the *cap6Δ* mutant but displayed a noticeable decrease

in MW with more smeared bands in the *ktr3Δ* mutant strain. The MP88 protein band of the *ktr3Δ cap6Δ* mutant migrated substantially faster than that of the WT and *ktr3Δ* strains. This strongly indicates that MP88 is highly modified by O-glycosylation by Ktr3, along with an additional contribution of Cap6, such that the extension of O-mannosylation is completely defective in the *ktr3Δ cap6Δ* strain.

To identify other protein targets to be highly O-mannosylated, we explored glycosylation patterns of the *C. neoformans* homologs of two *Saccharomyces cerevisiae* cell surface sensor proteins (Fig. 2B). The WSC family (Wsc1 to -4 proteins) and the Mid2p-Mtl1p pair sense environmental stresses in *S. cerevisiae*. These proteins are highly O-mannosylated within Ser/Thr-rich domains and are involved in the MAPK signaling pathway, activating cell wall synthesis to maintain cell wall integrity (40). These putative cell wall stress sensors were identified in the *C. neoformans* proteome through four sequential *in silico* analyses: (i) proteins containing a region of 40 amino acids in which the Ser/Thr content was  $\geq 40\%$  (958 proteins); (ii) proteins containing a single-pass transmembrane domain at the C-terminus (80 proteins); (iii) the presence of a signal peptide at the N-terminus without a GPI anchor domain (12 proteins); and (iv) the presence of putative O-glycosylation sites (2 proteins) (Fig. S3A). This analysis resulted in two putative cell wall sensors of *C. neoformans*, CNAG\_01255 and CNAG\_03328, each with a highly Ser/Thr-rich region subject to O-glycosylation. CNAG\_01255 and CNAG\_03328 are predicted to have 83 sites and 79 sites, respectively. Therefore, we named CNAG\_01255 Wml1 (*Wsc-Mid2-like 1*) and CNAG\_03328 Wml2 (*Wsc-Mid2-like 2*). The null mutants of cell wall stress sensors, *wml1Δ*, *wml2Δ*, and *wml1Δ wml2Δ* mutants, were constructed (Fig. S4) and analyzed for their growth phenotypes (Fig. S5A). Although the *wml1Δ*, *wml2Δ*, and *wml1Δ wml2Δ* mutant strains exhibited no detectable growth defects under other stress conditions, *wml2Δ* and *wml1Δ wml2Δ* mutant strains showed significantly increased sensitivity to salt stress caused by the presence of 1 M NaCl (Fig. S5A). The salt sensitivity to 1 M NaCl was also restored by 1 M sorbitol (Fig. S5B). The *wml1Δ* mutant has a very subtle defect in growth on salt, but the *wml1Δ wml2Δ* double mutant has a synthetic effect on growth on salt, indicating that both Wml1 and Wml2 play overlapping and partially redundant roles in the salt stress response.

In subcellular fractionation experiments, hemagglutinin (HA)-tagged Wml1 and Wml2 were mainly detected in the insoluble fraction (cell wall/membrane) (Fig. 2B). The Wml1 and Wml2 proteins were expressed as forms much larger ( $\geq 140$  kDa) than the predicted size (approximately 56 kDa) in the WT strain, suggesting extensive posttranslational modification. Moreover, the expression levels of Wml1 and Wml2 were different in the O-glycan-deficient *ktr3Δ*, *cap6Δ*, and *ktr3Δ cap6Δ* strains. The expression levels of Wml1 were decreased in the O-glycan-deficient strains, with a more dramatic decrease in the *cap6Δ* mutant than the *ktr3Δ* mutant, indicating that Wml1 is mainly subjected to minor O-mannosylation. In the *ktr3Δ cap6Δ* mutant strain, we could not detect the protein bands corresponding to Wml1 protein. In contrast, Wml2 proteins with lower MW accumulated more in the *ktr3Δ* mutant than in the *cap6Δ* mutant, suggesting that this protein is largely glycosylated by major O-mannosylation via Ktr3. Further decreased levels of Wml2 proteins in both high- and low-MW forms were detected in the *ktr3Δ cap6Δ* strain. This clearly indicates that O-linked glycans of Wml1 and Wml2 were differently modified by minor and major O-linked mannosylation, respectively. The signals for the protein bands of Wml1 and Wml2 were both greatly decreased in the *ktr3Δ cap6Δ* mutant (Fig. 2B), supporting that *C. neoformans* Wml1 and Wml2 are highly O-glycosylated at the Ser/Thr region, which is required for their stability.

**Extended mannosylation of O-linked glycans is essential for the adaptation responses to various external stress.** To assess the physiological impact of a complete block of extension of O-mannosylation, the WT and *ktr3Δ*, *cap6Δ*, and *ktr3Δ cap6Δ* mutant strains were cultivated on yeast extract-peptone-dextrose (YPD) plates under various stress conditions, including heat, osmotic, ER, and cell wall stresses (Fig. 3A and B). The *ktr3Δ* mutant, defective in major O-glycan biosynthesis, displayed increased sensitivity to high temperature (39°C), NaCl, tunicamycin (TM), calcofluor white (CFW), sodium dodecyl sulfate (SDS), and vanadate (VAN). In contrast, the *cap6Δ*

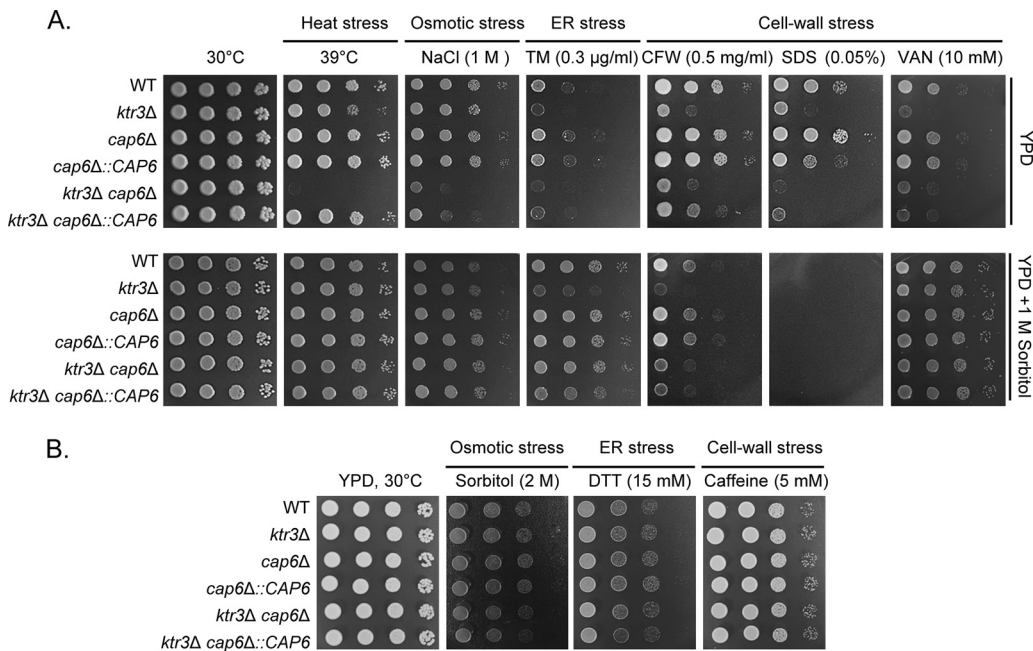


**FIG 3** Growth phenotypes of *C. neoformans* O-glycan mutant strains. (A) Growth analysis of *C. neoformans* O-glycan mutant strains with or without 1 M sorbitol under different conditions. Serially diluted cells were spotted on YPD plates with or without 1 M sorbitol under different conditions, including heat stress (39°C), ER stress (TM), cell wall stress (CFW, calcofluor white; SDS, sodium dodecyl sulfate; VAN, vanadate), and osmotic stress (NaCl). (B) Spotting analysis of growth of *C. neoformans* O-glycan mutant strains in the presence of DTT, caffeine, and sorbitol.

mutant, defective in minor O-glycan biosynthesis, did not display any detectable growth alteration under the tested stress conditions except SDS treatment. Interestingly, the *cap6Δ* mutant appeared to be slightly more resistant to SDS. The *ktr3Δ cap6Δ* double mutant exhibited increased sensitivity to high temperature, NaCl, and SDS compared to the *ktr3Δ* single mutant (Fig. 3A). Reintroduction of *CAP6* into the *ktr3Δ cap6Δ* mutant restored the growth defects at high temperature and in the presence of SDS to levels similar to those of the *ktr3Δ* mutant (Fig. 3A). Reintroduction of *KTR3* into the double mutant complemented more fully the growth phenotypes to levels similar to those of the *cap6Δ* strain (Fig. S2E). The growth defects of the *ktr3Δ cap6Δ* mutant under stress conditions, except CFW treatment, were also almost completely suppressed by the addition of 1 M sorbitol as an osmotic stabilizer, suggesting that the stress sensitivity of O-mannosylation mutants is mainly caused by defective cell wall integrity. In contrast, the *ktr3Δ* single mutant and even the *ktr3Δ cap6Δ* double mutant did not show increased sensitivity to 2 M sorbitol, dithiothreitol (DTT), or caffeine compared to the WT strain (Fig. 3B). Capsule formation and melanin synthesis in the O-mannosylation mutants did not differ significantly from those in the WT strain (Fig. S2F and G). These results suggest that the extended structure of the O-glycans in the Golgi apparatus, including major and minor O-glycans, is critical for the adaptative responses to several external stresses in *C. neoformans* but dispensable for capsule and melanin formation.

**O-Mannosylation plays a role in the Mpk1-cell wall integrity signaling pathway but not in the Hog1-salt stress signaling pathway.** We examined whether truncated O-mannosylation would generate defects in *C. neoformans* Mpk1- and Hog1-mediated stress signaling pathways. TM treatment was previously shown to induce phosphorylation of the CWI-controlling Mpk1 MAP kinase in *C. neoformans* (41) (Fig. 4A). Although the levels of phosphorylated Mpk1 decreased moderately in the *ktr3Δ* mutant and had no detectable change in the *cap6Δ* mutant, they markedly decreased in the *ktr3Δ cap6Δ* mutant compared to the WT upon TM treatment (Fig. 4A). The levels of phosphorylated Mpk1 were also markedly decreased in the *wml1Δ wml2Δ* double mutant compared to the WT upon TM treatment, even though there was no apparent decrease

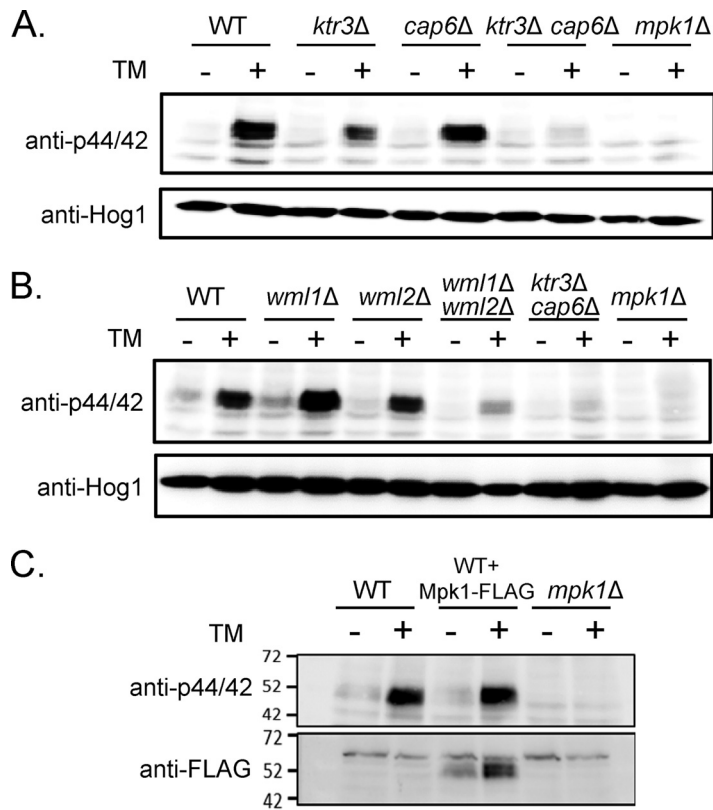


**FIG 4** Analysis of MAPK-mediated stress response signaling activity. (A and B) Phosphorylation of Mpk1 induced by TM in the WT, *O*-glycosylation mutants (*ktr3Δ*, *cap6Δ*, and *ktr3Δ cap6Δ* mutants), and cell wall stress sensor mutants (*wml1Δ*, *wml2Δ*, and *wml1Δ wml2Δ* mutants). Phosphorylated Mpk1 (Mpk1-p) was detected with phospho-p44/42-MAPK antibody, and Hog1 protein was detected with anti-Hog1 as a loading control, as described in Text S1 in the supplemental material. (C) Expression level of Mpk1 protein induced under the TM treatment condition. The pattern of phosphorylated Mpk1 (Mpk1-p) was detected with phospho-p44/42-MAPK antibody and Mpk1 protein with anti-FLAG.

in Mpk1 phosphorylation in the *wml1Δ* or *wml2Δ* single mutant strains (Fig. 4B). Mpk1 total protein levels also increased upon TM treatment (Fig. 4C). Taken together, these results suggest that defective *O*-mannosylation and the loss of the putative cell wall stress sensors Wml1 and Wml2 are important components in the translation of cell stress, such as TM-mediated ER stress, to the activation of the Mpk1-mediated CWI signaling pathway.

Since the Hog1 MAPK plays a role in maintaining osmotic balance, particularly under carbon-starved conditions (42), we compared osmotic stress response phenotypes under both glucose-rich and -starved conditions. Remarkably, the salt sensitivity of the *wml1Δ wml2Δ* double mutant was more severe than that of the *ktr3Δ cap6Δ* mutant and the *msb2Δ* mutant strain, which has a null mutation of *MSB2* encoding a mucin-like transmembrane protein involved in osmosensing (43), indicating that the Wml proteins play an important role in salt stress response (Fig. S5C). Interestingly, the *wml1Δ wml2Δ* and *ktr3Δ cap6Δ* double mutant strains displayed similar levels of osmosensitivity under both glucose-rich and -starved conditions, indicating that *O*-glycans play important roles in maintaining osmotic balance, which might be operated in a Hog1-independent manner (Fig. S5C). To further assess whether the contribution of *O*-glycans to osmoadaptation is associated with Hog1, we analyzed the Hog1 phosphorylation patterns in WT and *O*-glycan mutant strains in response to 1 M NaCl (Fig. S5D). In the WT strain, phosphorylated Hog1 was gradually dephosphorylated upon exposure to 1 M NaCl, as previously reported (44). A similar pattern of Hog1 dephosphorylation was also observed in the *ktr3Δ cap6Δ* and *wml1Δ wml2Δ* double mutant



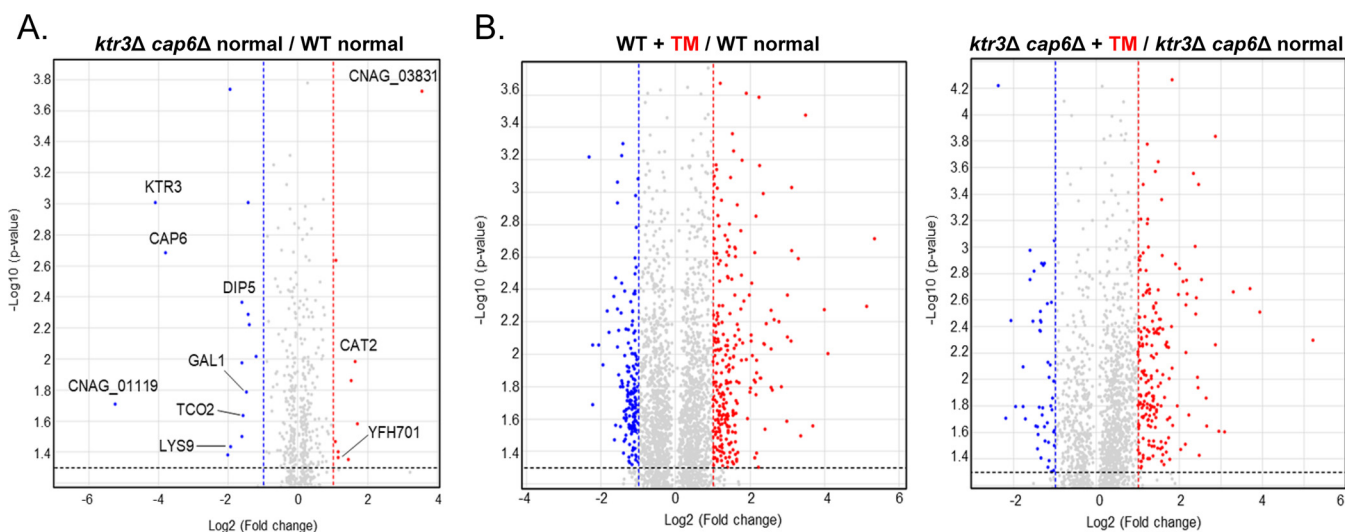


**FIG 5** Comparative RNA-Seq analysis of the WT and *ktr3Δ cap6Δ* strains. (A) Volcano plot comparing  $\log_2$  (2-fold change) values for the WT versus *ktr3Δ cap6Δ* strains under normal growth conditions. (B) Volcano plot comparing  $\log_2$  (2-fold change) values for the WT versus *ktr3Δ cap6Δ* strains upon tunicamycin (TM) treatment. *C. neoformans* WT and mutant cells at an  $OD_{600}$  of 0.15 were cultured in 50 mL of YPD broth at 30°C in a shaking incubator until the  $OD_{600}$  reached 0.8, the early phase of exponential growth. The cells were then treated with 5  $\mu\text{g}/\text{mL}$  TM and further incubated at 30°C in a shaking incubator for 1 h. Total RNA was extracted and subjected to RNA-Seq analysis as described in Text S1 in the supplemental material.

strains under osmotic stress by 1 M NaCl. This indicates that O-glycosylation is not required for Hog1 activation in response to osmotic/salt stress.

**Transcriptome analysis reveals defective Mpk1-mediated stress response signaling pathway in O-glycan mutants.** To elucidate regulatory networks with downstream components governed by O-mannosylation, we performed RNA sequencing (RNA-Seq)-based transcriptome analysis. The transcriptome profiles of the WT and *ktr3Δ cap6Δ* cells treated with TM (5  $\mu\text{g}/\text{mL}$ ) for 1 h were compared to those without TM treatment. First, we analyzed the genes that were differentially expressed more than 2-fold between the WT and *ktr3Δ cap6Δ* cells cultivated in YPD medium (Fig. 5A). Under this permissive growth condition, *CAT2* (catalase 2) and CNAG\_03831 (unknown function) were highly upregulated in the *ktr3Δ cap6Δ* mutant compared to those in the WT strain, while the genes involved in transmembrane transport, such as CNAG\_01119 encoding a POT family proton-dependent oligopeptide transporter, were significantly downregulated (Fig. 5A; Fig. S6A) in the *ktr3Δ cap6Δ* mutant compared to those in the WT.

We next analyzed the differential gene expression pattern between the WT and *ktr3Δ cap6Δ* mutant upon TM treatment. We found that fewer genes showed changes in their expression levels in the *ktr3Δ cap6Δ* mutant than in the WT after TM treatment (Fig. 5B). In the WT strain, the expression of 423 genes (260 upregulated, 163 downregulated) was altered at least 2-fold in the presence of TM. In contrast, in the *ktr3Δ cap6Δ* mutant, 241 genes (193 upregulated, 48 downregulated) showed differential expression upon TM treatment (Fig. S6B). Those genes involved in the ER stress response mediated by the unfolded protein response (UPR) signaling pathway, such as genes involved in protein folding, glycosylation, and proteolysis (41), were induced upon TM treatment in both the WT and the *ktr3Δ cap6Δ* mutant but with slightly more upregulated genes in the *ktr3Δ cap6Δ* mutant (data not shown). The differential gene expression patterns were also reflected in the enrichment scores of DAVID analysis, additionally indicating that the small GTPase-mediated signal transduction category was upregulated in the WT upon TM treatment but not in the *ktr3Δ cap6Δ* mutant (Fig. S6C). Our transcriptome data also indicated that a set of genes in the calcineurin-Crz1 pathway (calcineurin-responsive zinc finger 1), which is coordinately regulated by phosphorylated Mpk1 in *S. cerevisiae* (45) and in *C. neoformans* (46), were upregulated by TM treatment in the *C. neoformans* WT strain but not in the *ktr3Δ cap6Δ* strain (data not shown). We further validated our transcriptome data by quantitative reverse

transcription-PCR (qRT-PCR) analysis (Fig. S7A and B), strongly supporting that the blockage of *O*-glycan extension in the *ktr3Δ cap6Δ* strain results in defective Mpk1-mediated stress response signaling pathways.

**Truncation of both major and minor *O*-glycans completely abolishes virulence in *C. neoformans*.** In our previous study, the truncation of the major *O*-glycans by the *KTR3* deletion was shown to severely attenuate virulence in animal models of *C. neoformans* infection (31). To assess the effect of an additional block of the extension of minor *O*-glycans on pathogenicity, we compared the virulence of *cap6Δ*, *ktr3Δ*, and *ktr3Δ cap6Δ* mutant strains to that of the WT in a murine inhalational model of systemic cryptococcosis. Although the single deletion of *CAP6* did not cause a detectable decrease in virulence of *C. neoformans*, the *ktr3Δ cap6Δ* mutant was more severely virulence attenuated than the *ktr3Δ* mutant. Even at 60 days postinfection (dpi), none of the mice infected with the *ktr3Δ cap6Δ* strain showed signs of clinical illness. Reintroduction of the WT *CAP6* gene into the *ktr3Δ cap6Δ* mutant restored virulence to the degree of the *ktr3Δ* mutant, indicating that the extended structures of both major and minor *O*-glycans contribute additively to the full pathogenicity of *C. neoformans*, although the role of minor *O*-glycans is not critical for virulence in the presence of major *O*-glycans (Fig. 6A).

Analysis of the lungs by quantitative culture at 21 dpi showed a marked decrease in fungal burden for the *ktr3Δ cap6Δ* strain compared to that of the WT and *ktr3Δ cap6Δ::CAP6* strains (Fig. 6B, top panel). Dissemination to the brain was also markedly reduced for both the *ktr3Δ cap6Δ* and *ktr3Δ cap6Δ::CAP6* strains, suggesting that *O*-glycans with extended structures are important for *C. neoformans* survival and proliferation in host environments after host infection. Histopathological analysis of mucicarmine-stained polysaccharide capsule of *C. neoformans* further supported the complete abolishment of the *ktr3Δ cap6Δ* cells in contrast to the extensive proliferation of the WT *C. neoformans* and a few surviving *ktr3Δ cap6Δ::CAP6* cells in the lung tissues (Fig. 6C, upper panel). In the brain tissues, a small number of *C. neoformans* cells was observed only in animals infected with the WT (Fig. 6C, lower panel).

**Extended *O*-glycans are required for host cell interaction in sequential steps of infection.** We defined the sequential infection steps involving *O*-glycan-mediated microbe-host interactions by analyzing the nature of the interaction of *C. neoformans* *O*-glycan mutant strains with lung epithelial cells, macrophage-like cells, and brain microvascular endothelial cells (Fig. 7). As the first step of host interaction during infection, we examined the efficiencies of adhesion of *O*-mannosylation mutant strains to A549 lung epithelial cells. The *ktr3Δ*, *ktr3Δ cap6Δ*, and *ktr3Δ cap6Δ::CAP6* strains showed significant reductions in epithelial cell adhesion efficiency, while the *cap6Δ* strain did not display apparent changes compared to the WT strain (Fig. 7A). For the subsequent infection step, we analyzed the uptake efficiency of *C. neoformans* mutant cells by macrophage-like cells (J774A.1) (Fig. 7B, left). The opsonic phagocytosis rates after 1 h of host-fungal cell coinubation were similar between WT and *O*-mannosylation mutant cells, indicating that the uptake efficiency by macrophages, the early step of phagocytosis, was not compromised by truncated *O*-glycans. To investigate the proliferation capability of the *C. neoformans* cells within the macrophage as a subsequent step of phagocytosis, we compared the intramacrophage survival capacities of WT and *O*-glycan mutant strains. The number of *C. neoformans* cells surviving within macrophages was remarkably reduced for the *ktr3Δ cap6Δ* mutant strain compared to the WT (~50%) (Fig. 7B, right). A more severely decreased survival capacity was observed in the *ktr3Δ cap6Δ* double mutant strain than the *ktr3Δ* single mutant, supporting the additive effect of minor *O*-mannosylation on *C. neoformans* intracellular survival.

Our recent study on genome-wide functional analysis of *C. neoformans* phosphatases indicated the involvement of the Golgi membrane-bound apyrases, *Gda1* and *Ynd1*, in the interactions with the blood-brain barrier (BBB) (47). It was hypothesized that *Gda1* and *Ynd1* could modulate the mannosylation of both *N*-linked and *O*-linked glycoproteins as well as the addition of mannose residues to glycosphingolipids by affecting the antiport exchange ratio between GDP-mannose and GMP. To further

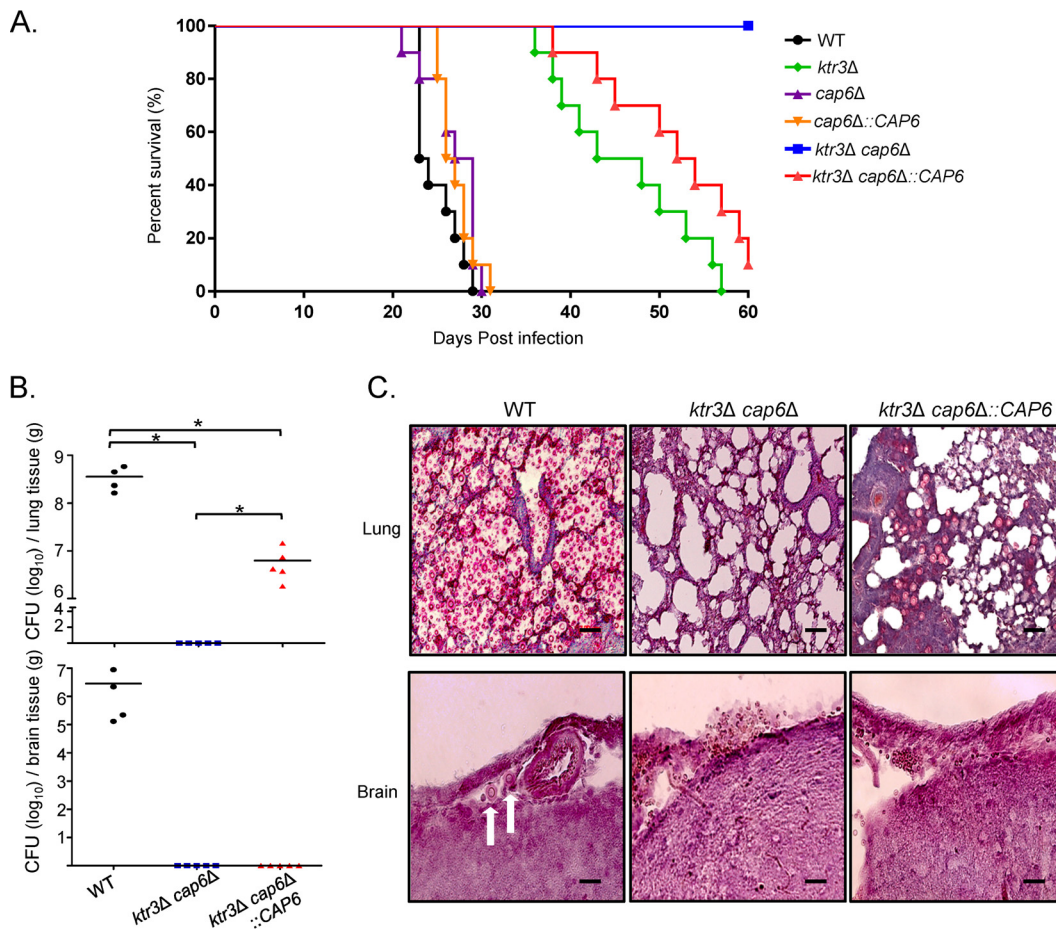


**FIG 6** *In vivo* analysis of virulence of *C. neoformans* O-glycan mutants. (A) Survival analysis of mice infected *C. neoformans*. A/Jcr mice were infected with  $10^5$  cells of WT, *ktr3Δ*, *cap6Δ*, *cap6Δ::CAP6*, *ktr3Δ cap6Δ*, and *ktr3Δ cap6Δ::CAP6* strains by intranasal instillation. Survival (%) was monitored for 8 weeks postinfection. (B) CFU of *C. neoformans* in the tissues of infected mice. The numbers of CFU per gram of lung and brain tissues were determined upon sacrifice of the mice infected with WT, *ktr3Δ cap6Δ*, and *ktr3Δ cap6Δ::CAP6* cells at day 21. \*,  $P < 0.05$  for WT versus *ktr3Δ cap6Δ* mutant, WT versus *ktr3Δ cap6Δ::CAP6* mutant, and *ktr3Δ cap6Δ* mutant versus *ktr3Δ cap6Δ::CAP6* mutant by one-way analysis of variance and Bonferroni's *post hoc* tests. (C) Histopathological staining of infected lung and brain tissues with mucicarmine. White arrows indicate *C. neoformans* cells.

investigate the requirement of O-linked glycoproteins for the interaction with the BBB, we compared the abilities of the *ktr3Δ cap6Δ* double mutant and WT cells to adhere to and cross cells associated with the BBB. We used an established *in vitro* transcytosis system, which consists of a transwell membrane coated with human cerebral microvascular endothelial cells (hCMEC/D3) separating a top compartment (blood side) and a bottom compartment (brain side) (48). Negative controls included *C. neoformans* strains with known defects in BBB penetration: (i) the *mpr1Δ* metalloprotease mutant (a brain infection-related factor that alters endothelium permeability [49]) and (ii) the *ssu72Δ* and *gda1Δ* phosphatase mutants (47). The O-glycan *ktr3Δ* and *ktr3Δ cap6Δ* mutant strains did not show any decreased ability of adhesion to the hCMEC/D3 cells. Notably, however, they showed a significantly reduced ability to traverse the BBB, suggesting that protein O-mannosylation is required for the full activity of BBB crossing but not adhesion to brain endothelial cells (Fig. 7C).

**Truncated O-glycans are defective in stimulating host immune response and in inducing host cell lysis.** Dendritic cells are among the first immune cells that *C. neoformans* contacts in the infected lungs (50). To investigate whether the truncated O-glycans of the *ktr3Δ cap6Δ* mutant affect the response of host immune cells, we quantified the production of the proinflammatory cytokines tumor necrosis factor

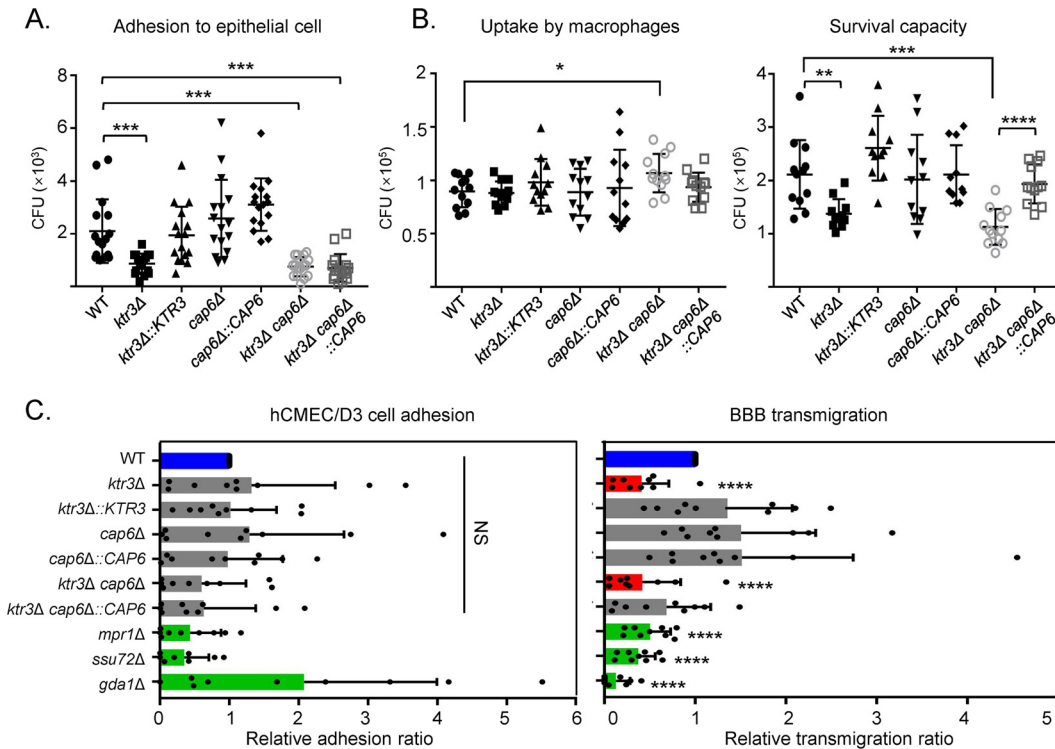


**FIG 7** *In vitro* analysis of the interaction of *C. neoformans* O-glycan mutant strains with host cells. (A) Analysis of adherence to A549 (lung epithelial cells). The numbers of CFU of *C. neoformans* cells recovered from host cell lysates were counted after coincubation of *C. neoformans* cells with A549 lung epithelial cells at 37°C with 5% CO<sub>2</sub> for 1 h. (B) Analysis of uptake by macrophages and survival capacity of *C. neoformans* in murine macrophage J774A.1. Opsonized *C. neoformans* cells were incubated with activated J774A.1 macrophages for 1 h. The numbers of CFU were counted to determine early phagocytosis. Survival capacity of *C. neoformans* by macrophages was determined by counting CFU in lysed macrophages. (C) Brain cell (hCMEC/D3) adhesion and BBB transmigration assays. Left panel, analysis of adherence to hCMEC/D3 cells. The numbers of CFU of *C. neoformans* cells recovered from host cell lysates were counted after coincubation of yeast cells with hCMEC/D3 at 37°C with 5% CO<sub>2</sub> for 1 h. Right panel, analysis of transmigration assay. hCMEC/D3-coated plates were inoculated with yeast cells and incubated at 37°C in a CO<sub>2</sub> incubator for 24 h, and the number of yeast cells passing through the hCMEC/D3-coated transwell was measured by CFU. *C. neoformans mpr1Δ*, *ssu72Δ*, and *gda1Δ* mutants were used as negative controls. x axes indicate the relative ratios of adhesion and transmigration, respectively. Each mutant was analyzed by three biologically independent experiments with three technical replicates. Data are presented as the mean value ± standard error of the mean (SEM). Statistical significance of differences between the WT (H99 strain) and each mutant (\*\*\*\*, *P* < 0.0001) was calculated by a two-tailed Student's *t* test.

alpha (TNF- $\alpha$ ) and interleukin 6 (IL-6) from bone marrow-derived dendritic cells (BMDCs) after *C. neoformans* infection. The BMDCs were coincubated with *C. neoformans* cells for 12 h, and the levels of cytokines from the cell culture supernatant were assayed (Fig. 8A). All strains were created in the *cap59Δ* background to minimize the antiphagocytic effect of the surface capsule, as performed previously (39). The BMDCs infected with either *ktr3Δ* or *ktr3Δ cap6Δ* mutant cells secreted lower levels of TNF- $\alpha$  and IL-6 during coincubation than those infected with the WT and *cap6Δ* cells. Interestingly, the *ktr3Δ::KTR3* complementation strain induced increased cytokine secretion compared with the WT, possibly due to the altered expression of reintroduced *KTR3*, which might generate O-glycan profiles that are not exactly the same as those of the WT (Fig. S2D).

Previous studies suggested that host cell pyroptosis, a cell escape strategy employed by fungal pathogens, is triggered by the O-mannosylated proteins assembled on the fungal cell surface (22–24). To examine whether defective O-mannosylation in *C. neoformans* also affects pyroptosis, we measured the levels of lactate dehydrogenase (LDH) and IL-1 $\beta$  released from BMDCs after 3 h, 6 h, and 16 h of coincubation with *C. neoformans* cells, including the WT, O-glycosylation mutants, and the *alg3Δ* N-glycosylation mutant strain (Fig. 8B). As previously reported for BMDCs infected with WT *C.*

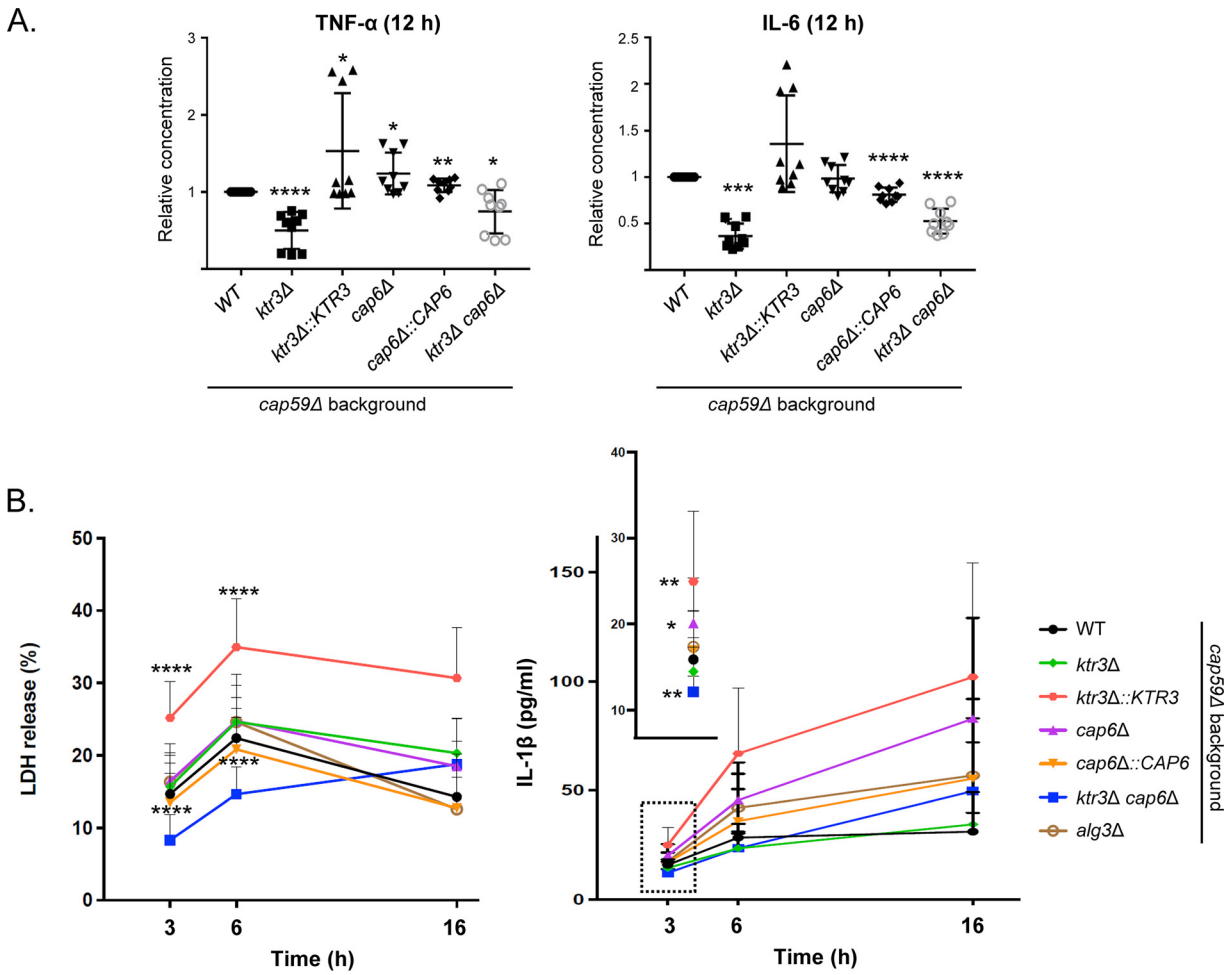


**FIG 8** *In vitro* analysis of host immune response upon *C. neoformans* infection. (A) Analysis of cytokine secretion from host dendritic cells. *C. neoformans* cells were cocultivated with BMDCs for 12 h, and the levels of TNF- $\alpha$  and IL-6 secreted from dendritic cells were measured. Data represent means of triplicates from three independent experiments ( $n = 9$ ). y axes indicate the relative concentrations of cytokines, which were calculated relative to those of the *cap59Δ* mutant. All the statistical analyses were performed using an unpaired two-tailed Student's *t* test (\*,  $P < 0.05$ ; \*\*,  $P < 0.01$ ; \*\*\*,  $P < 0.001$ ; \*\*\*\*,  $P < 0.0001$ ). (B and C) Analysis of host cell lysis and IL-1 $\beta$  release from BMDCs. BMDCs from WT mice were infected with cells of the WT, *O*-glycan mutants, and *alg3Δ* mutant in an acapsular background for the indicated times (3 h, 6 h, and 16 h). The cell culture supernatants were collected and assayed for LDH and IL-1 $\beta$  via ELISA (\*,  $P < 0.05$ ; \*\*,  $P < 0.01$ ; \*\*\*,  $P < 0.001$ ; \*\*\*\*,  $P < 0.0001$ ).

*neoformans*, LDH release showed almost the maximum value at 6 h without further increase while IL-1 $\beta$  release increased with prolonged incubation time (39). In contrast to the incubation with the *alg3Δ* mutant carrying truncated *N*-glycans, the BMDCs infected with the *ktr3Δ cap6Δ* mutant strain carrying truncated *O*-glycans showed reduced release of both LDH and IL-1 $\beta$ . However, the decreased release of IL-1 $\beta$  was evident only after 3 h of coinubation with the *ktr3Δ cap6Δ* strain, suggesting that *O*-glycans of *C. neoformans* are partly involved in triggering pyroptosis, which appears to occur early during infection (Fig. 8B). At later stages of coinubation (16 h), both LDH and IL-1 $\beta$  levels in the BMDCs infected with the *ktr3Δ cap6Δ* mutant were increased almost to the levels seen with the incubation with the WT *C. neoformans* cells (Fig. 8B), indicating that nonpyroptotic host cell lysis occurs at the late stage of infection without association with *O*-mannosylation.

Previous studies strongly indicated that *O*-mannosylation of cell wall mannoproteins plays a role in cell surface localization of ergosterol, which is important for the ability of *S. cerevisiae* and *C. albicans* to trigger pyroptosis (24, 51). To examine the effects of altered ergosterol localization in our *O*-mannosylation extension mutants, we stained the *ktr3Δ*, *cap6Δ*, and *ktr3Δ cap6Δ* mutants with filipin, a naturally fluorescent

polyene antibiotic that binds to ergosterol, and analyzed them by fluorescence microscopy (Fig. 9A). Whereas the WT cells showed uniform staining of the plasma membrane (PM) (Fig. 9Aa), the *ktr3Δ cap6Δ* cells exhibited a pattern of scattered cytoplasmic and cell surface puncta (Fig. 9Af), resulting in significantly reduced cellular fluorescence signal at the PM. The *cap6Δ* and *ktr3Δ* single mutant strains showed an intermediate pattern of filipin staining between that of the WT and the *ktr3Δ cap6Δ* double mutant (Fig. 9Ab and d). The defects in ergosterol localization at the PM in the *ktr3Δ cap6Δ* strain were restored, accompanied by the disappearance of filipin-stained puncta, by complementation with either *CAP6* and *KTR3* (Fig. 9Ac, e, g, and h), as assessed by quantifying the percentage of cells with puncta.

We further investigated whether such altered ergosterol distribution might be associated with defective ergosterol biosynthesis by comparing the total fluorescence intensities of filipin staining (Fig. 9B) and the sterol profiles based on HPLC analysis (Fig. 9C). There was no apparent difference in total fluorescence intensity among WT and *O*-mannosylation mutant cells (Fig. 9B), indicating that total ergosterol levels were not detectably different between WT and *O*-mannosylation-defective strains. Considering that sterols are synthesized from the ER and transported, presumably by sterol transport proteins, to the sterol-enriched PM primarily via nonvesicular intracellular sterol pathways (52), we prepared sterol samples by employing the KOH-heptane extraction procedure, which is used frequently for measurement of total intracellular ergosterol production in fungal cells (53). When total intracellular sterol samples were analyzed by HPLC, the sterol profiles did not show notable difference between the WT, *ktr3Δ cap6Δ*, *ktr3Δ cap6Δ::KTR3*, and *ktr3Δ cap6Δ::CAP* strains (Fig. 9C). These nearly equivalent sterol profiles by HPLC analysis indicated that the *O*-mannosylation mutants do not have a defect in ergosterol biosynthesis. This suggests that the altered distribution of ergosterol observed by fluorescence microscopy likely results from defective trafficking of ergosterol. Abnormal ergosterol distribution was most notably observed in the *ktr3Δ cap6Δ* strain cultivated under host-mimicking conditions (TC medium, 37°C) (Fig. 9D).

## DISCUSSION

Protein *O*-mannosylation is a highly conserved process among eukaryotes by which PMTs in the ER catalyze the addition of mannose residues to Ser/Thr residues of their protein substrates (2). The further processing of *O*-mannosylation in the Golgi apparatus is differentially regulated in a species-specific manner, generating *O*-glycans with different structures and composition. In most yeasts studied thus far, the first mannose  $\alpha$ -linked to Ser/Thr residues may be extended to form an  $\alpha$ 1,2-linked mannotriose (Man $\alpha$ 1-2Man $\alpha$ 1-2Man $\alpha$ 1-Ser/Thr). This core structure is further processed differently according to the yeast species but mostly by the addition of mannose residues. The structures of the *C. neoformans* *O*-glycans are quite distinctive from those of other fungi, in that Man $\alpha$ 1-2Man $\alpha$ 1-6-Man $\alpha$ 1-2Man mannotetraose is generated as major *O*-glycans by attaching the third mannose via  $\alpha$ 1,6-linkage instead of  $\alpha$ 1,2-linkage in *C. neoformans*, which is mediated by Hoc3, an  $\alpha$ 1,6-mannosyltransferase (31). Interestingly, *C. neoformans* also has oligomannoses containing xylose, Xyl<sub>1</sub>Man<sub>2</sub> to Xyl<sub>1</sub>Man<sub>4</sub> (X1M2 to X1M4), as minor *O*-linked glycans (Fig. 1B). We previously reported that the second  $\alpha$ 1,2-linked mannose residue in the major *O*-glycans is added to the first mannose by Ktr3 (31). Here, we demonstrated that Cap6, which was previously identified as  $\alpha$ 1,3-mannosyltransferase based on its homology to Cap59 involved in capsule biosynthesis, is responsible for the addition of the second mannose residue in  $\alpha$ 1,3-linkage, generating the minor *O*-glycans to be modified by addition of xylose. The subsequent addition of a third mannose in  $\alpha$ 1,6-linkage to minor *O*-glycans is mediated by Hoc1, another  $\alpha$ 1,6-mannosyltransferase, independently from major *O*-glycan biosynthesis in *C. neoformans* (31).

In *S. cerevisiae*, five membrane-spanning sensors, including Wsc1-3, Mid2, and Mtl2, detect external stress and trigger signal transduction cascades to maintain cell wall

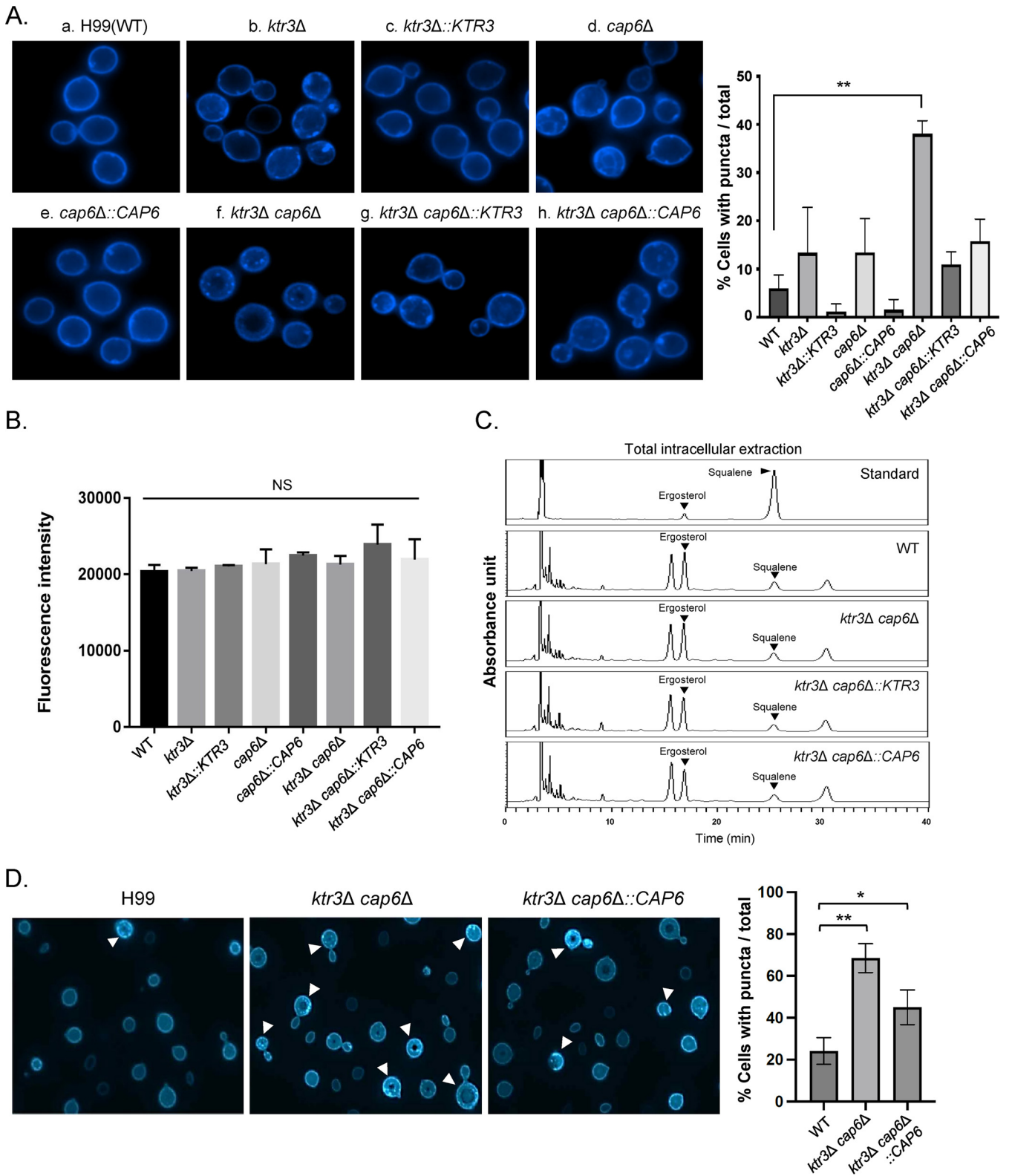


**FIG 9** Localization and quantification of ergosterol in *C. neoformans* O-glycan mutant strains. (A) Filipin staining analysis of ergosterol localization. *C. neoformans* WT, O-mannosylation mutant, and complementation strains were incubated for 6 h at 30°C in YPD medium, fixed and stained with 10 μg/mL filipin, and monitored by a fluorescence microscope. Fluorescence images are shown of WT (a), *ktr3Δ* (b), *ktr3Δ::KTR3* (c), *cap6Δ* (d), *cap6Δ::CAP6* (e), *ktr3Δ cap6Δ* (f), *ktr3Δ cap6Δ::KTR3* (g), and *ktr3Δ cap6Δ::CAP6* (h) strains. The percentage of cells with puncta among the total cell population is shown. (B) Total fluorescence intensity of filipin staining. Fluorescence levels were quantitatively measured at a 485-nm wavelength using a fluorescence microplate reader (BioTek, Winooski, VT, USA). Data represent means of triplicates from two independent experiments. (C) HPLC profiles of the sterol samples from WT, *ktr3Δ* (Continued on next page)

integrity. The structure of cell wall sensors has similar features, including a single trans-membrane domain and cytoplasmic tails. The serine/threonine-rich (STR) region is especially highly *O*-glycosylated, and it is stretched by external stress and triggers activation of the CWI signaling pathway (40). In this study, we identified two novel cell wall stress sensors via *in silico* analysis in *C. neoformans*, Wml1 and Wml2 (see Fig. S3A in the supplemental material), which are modified independently by two different *O*-glycan synthesis pathways: Wml1 was mostly subject to Cap6-mediated *O*-mannosylation, while Wml2 was modified mainly by Ktr3-mediated *O*-mannosylation (Fig. 2B). Unlike with the fungal pathogens *C. albicans* and *A. fumigatus*, the *C. neoformans* cell wall sensors have not yet been reported, except that CNAG\_03308 was previously predicted as a ScMtl1/ScMid2 homolog based on Pfam domain analysis (54). It is notable that *C. neoformans* Wml1 and Wml2 do not have the WSC1 domain or the MID2 domain, which are present in the cell wall sensors of other yeast species, including *S. cerevisiae* (Wsc1, Wsc2, Wsc3, Mid2, and Mtl2), *C. albicans* (Wsc1 and Wsc2), and *Schizosaccharomyces pombe* (Wsc1 and Mtl2) (Fig. S3B). Phylogenetic analysis revealed that the yeast Wsc and Mid proteins diverged from a common ancestor and evolved as a separate subfamily. It appears that *C. neoformans* Wml1 and Wml2 also evolved independently as a distinctive subfamily separated from other Wsc and Mid/Mtl homologs (Fig. S3C). *C. neoformans* Wml1 and Wml2 showed about 16% sequence identity to other cell wall stress sensors of several different yeasts (Fig. S3D), reflecting the difficult *in silico* identification based on sequence homology.

We observed decreased phosphorylation of Mpk1 in the *wml1Δ wml2Δ* mutant strain upon TM treatment, suggesting the involvement of Wml1 and Wml2 as cell surface sensors in inducing CWI signaling in response to external stress (Fig. 4B). It is notable that the loss of Wml2 resulted in highly increased sensitivity to 1 M NaCl (Fig. S5B); in contrast, the *wml1Δ*, *wml2Δ*, and *wml1Δ wml2Δ* mutant strains exhibited no detectable growth defects under other stress conditions (Fig. S5A). Considering that Wml2 is *O*-mannosylated, which is required for its stability (Fig. 2B), the high salt sensitivity of *ktr3Δ* and *ktr3Δ cap6Δ* mutant strains might be partly attributed to the altered structures of *O*-glycans assembled on Wml2 (Fig. 2B). Hog1 phosphorylation and dephosphorylation patterns were not affected in the *ktr3Δ cap6Δ* mutant strain, indicating that the Wml2 serves as a sensor responding to salt stress independently from the HOG pathway (Fig. 10A). Further identification and functional characterization of *C. neoformans* cell surface sensors would provide in-depth insights into the *C. neoformans* signal processing in response to stresses, about which only limited information has been available on the cell surface sensors so far.

We observed that TM treatment evidently repressed expression of ribosomal protein genes in the WT, as previously reported in *S. cerevisiae* (55), but to a lesser extent than that in the *ktr3Δ cap6Δ* mutant (Fig. S6C). TORC1 (target of rapamycin complex 1), the central stress and growth controller, is involved in activation of ribosomal biogenesis (56). A recent study in *S. cerevisiae* reported that the TORC1 pathway is inhibited by TM exposure in cells of the WT strain but not in those lacking Slr2 (Mpk1), indicating that Mpk1 is required to activate the ER stress-protective mechanism through TORC1 inhibition (57). It was previously reported that Mtl1 *O*-mannosylation mediated by both Pmt1 and Pmt2 was important for cell survival under oxidative conditions and TOR blockade in *S. cerevisiae* (58). The *C. neoformans ktr3Δ cap6Δ* mutant also showed increased sensitivity to rapamycin (Fig. S7C). Together, the results suggest that the defective *O*-mannosylation in *C. neoformans* resulted in less efficient TORC1 inhibition upon TM treatment partly due to defective Mpk1 activation, which plays a role in inducing the ER stress-protective response by inhibiting TORC1 (Fig. 10A).

As major components of the fungal cell wall and PM, glycoproteins contribute to

#### FIG 9 Legend (Continued)

*cap6Δ*, *ktr3Δ cap6Δ::KTR3*, and *ktr3Δ cap6Δ::CAP6* strains. For the separation of ergosterol by HPLC, the proportion of solvent A (95% acetonitrile [ACN]) was maintained at 100% for 40 min. (D) Filipin staining analysis of *C. neoformans* WT, *ktr3Δ cap6Δ*, and *ktr3Δ cap6Δ::CAP6* strains cultivated for 18 h under host-mimicking tissue culture conditions, in which *C. neoformans* cells were incubated in CO<sub>2</sub>-independent tissue culture medium (TC medium; Gibco) with shaking at 37°C. The arrowheads indicate the *C. neoformans* cells showing increased cytoplasmic puncta.



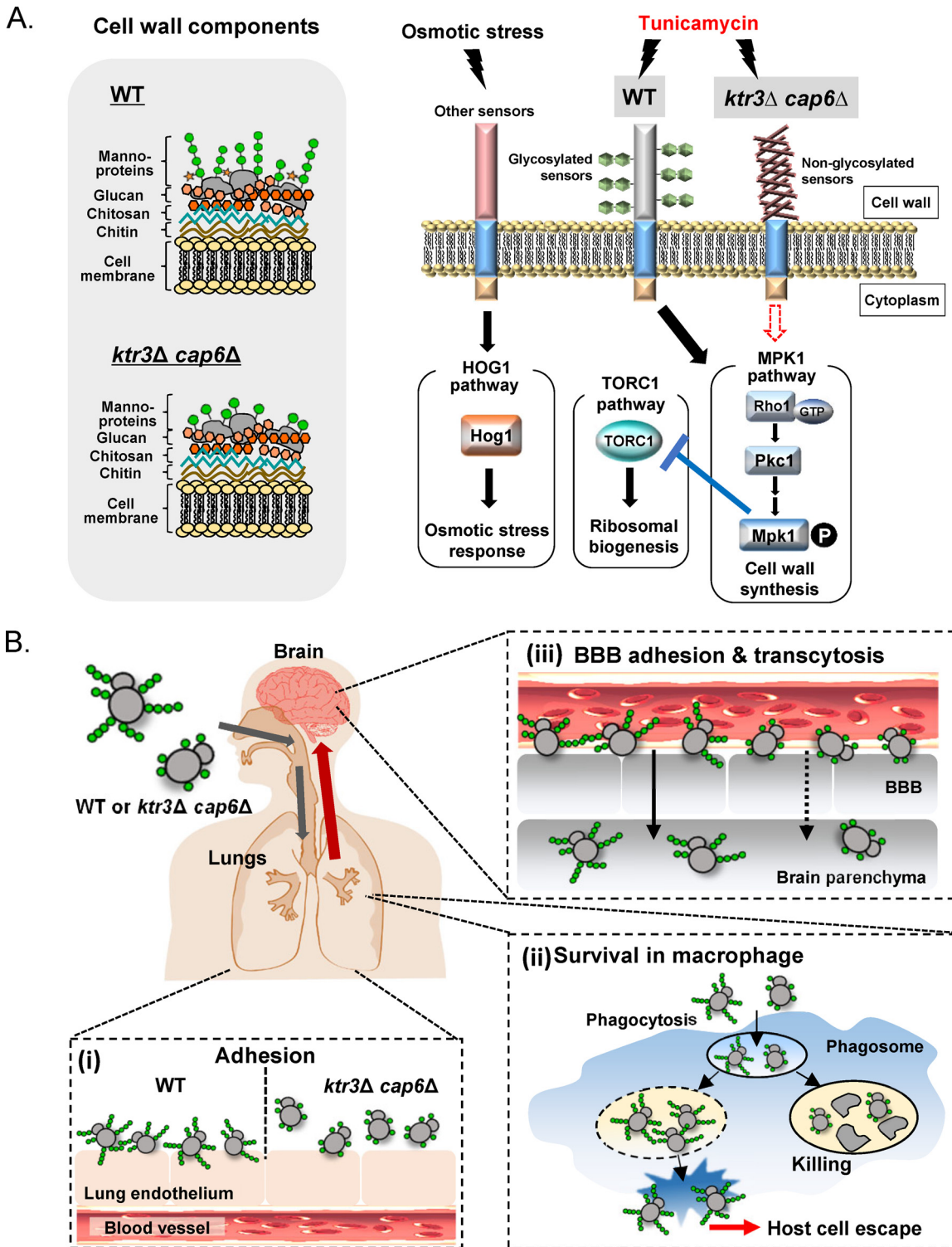


**FIG 10** Schematic summary of the CWI pathway and interaction with host cells of *C. neoformans* WT and *ktr3Δ cap6Δ* mutant. (A) Schematic representation of the stress response signaling pathways mediated by Mpk1, Hog1, and TORC1. Extended O-mannosylation of cell surface sensors is required to induce Mpk1-mediated CWI signaling pathways and to repress TORC1 pathway but not for the induction of the HOG pathway. (B) Representative key steps in host cell-*C. neoformans* interactions. The extension of O-mannosylation in the Golgi apparatus generated is important for the interaction with host cells from early lung infection to late brain invasion, including (i) adherence to lung epithelial cells, (ii) survival in macrophage and host cell lysis, and (iii) transmigration to BBB.

fungal pathogenicity and recognition by the host immunity (20). In our previous work on the *N*-glycosylation of *C. neoformans*, we reported that although the outer mannose chains of *N*-glycans are dispensable for the virulence of *C. neoformans*, an intact core *N*-glycan structure is required for *C. neoformans* pathogenicity (34, 39). The *C. neoformans* *ALG3*, *ALG9*, and *ALG12* deletion mutant strains, generating truncated core *N*-glycans, do not show defects in early stages of host cell interaction during infection, including attachment to lung epithelial cells, opsonic/nonopsonic phagocytosis, and phagosome maturation. However, the mutants defective in the core *N*-glycan biosynthesis exhibit decreased activity in inducing host cell death after phagocytosis, which is triggered as a mechanism of pulmonary escape and dissemination of *C. neoformans*, thus becoming inactive in causing fatal infection (39). Here, we presented a set of data indicating that the extended structure of *O*-glycans, generated by the Ktr3- or Cap6-mediated addition of the second mannose residue to the first mannose attached to target proteins in the Golgi apparatus, is important for proper interaction of *C. neoformans* with host cells at several steps during host infection (Fig. 10B). The *ktr3Δ cap6Δ* mutant showed decreased adhesion to lung epithelial cells, proliferation within macrophages, and reduced BBB crossing but normal efficiency of uptake by macrophages (Fig. 7). The *ktr3Δ cap6Δ* mutant also exhibited apparently reduced activity in inducing the immune response of primary host immune cells to secrete cytokines (Fig. 8). Particularly, the reduced release of both LDH and IL-1 $\beta$  from BMDCs upon infection with the *ktr3Δ cap6Δ* mutant indicates that cryptococcal *O*-glycans assembled on cell surface mannoproteins contribute to host cell pyroptosis, a cell escape strategy employed by fungal pathogens, although other factors are also required for full induction of host cell pyroptosis in *C. neoformans*. We observed the defective trafficking of ergosterol, which is considered an immunoreactive fungal molecule to trigger host cell pyroptosis (51), in the *ktr3Δ cap6Δ* cells (Fig. 9). Combined with the decreased resistance to stresses generated by host cell environments, the inefficient host cell escape of *ktr3Δ cap6Δ* cells could result in completely abolished virulence in *C. neoformans* (Fig. 10).

Besides decreased ergosterol localization in the plasma membrane of the *ktr3Δ cap6Δ* mutant strain, we examined the possibility that the defective *O*-glycan structure might induce altered physiochemical properties of the cell surface by changing other cell wall components (Fig. S8). Although no apparent difference in the total amount and overall lengths of *N*-glycans was observed between the WT and *ktr3Δ cap6Δ* mutant, the *N*-glycan profile of the *ktr3Δ cap6Δ* mutant showed decreased neutral glycan peaks ( $P = 0.0558$ ) with increased acidic glycan peaks ( $P = 0.0553$ ) compared to that of the WT strain (Fig. S8A and S8B). We observed a slightly increased amount of chitin (Fig. S8C) in the *ktr3Δ cap6Δ* mutant, which might reflect the compensation mechanism of defective cell wall integrity. Thus, the defective host interaction observed in the *ktr3Δ cap6Δ* mutant might result mainly from the combined effect of the truncated structure of *O*-glycans, which might be directly recognized with host glycan-binding proteins and the defective localization of ergosterol, which is required for triggering host immune response. Further studies to elucidate the underlying mechanisms on how the specific structures of *C. neoformans* *O*-glycans are recognized by host cells and how *O*-glycans are involved in ergosterol trafficking would facilitate our understanding of the glycan-based modulation of host-pathogen interactions in infectious fungi.

This study demonstrated the critical roles of *O*-glycan structures in the pathogenicity of *C. neoformans*. Even though PMT family inhibition is a possible strategy to block the initiation of *O*-glycan assembly on proteins, the PMT family is highly conserved through eukaryotes from yeast to *Homo sapiens*, and there is no single Pmt inhibitor with activity against all the PMT family enzymes on their diverse acceptor protein substrates. In contrast, there is no human homolog for the fungal mannosyltransferases working in the Golgi apparatus, such as *C. neoformans* Cap6 and Ktr3. Furthermore, the addition of the second mannose residue by Ktr3 and Cap6 in the Golgi apparatus occurs commonly in all the acceptor proteins subjected to *O*-mannosylation. Thus, the

fungus-specific  $\alpha$ 1,3-/ $\alpha$ 1,2-mannosyl transferases involved in O-mannosylation might be very promising targets for the development of new antifungal agents.

## MATERIALS AND METHODS

**Strains, media, plasmids, and primers.** The *C. neoformans* strains constructed and used in this study are listed in Table S1A in the supplemental material. Yeast cells were generally cultured in YPD medium (1% [wt/vol] yeast extract, 2% [wt/vol] peptone, 2% [wt/vol] dextrose) with shaking (220 rpm) at 30°C. The plasmids and primers used in this study are listed in Tables S1B and C, respectively. *C. neoformans* transformants were selected on YPD solid medium containing 100  $\mu$ g/mL nourseothricin acetyltransferase (Jena Bioscience), referred to here as YPD<sub>NATr</sub>, or on YPD solid medium containing 200  $\mu$ g/mL G418 disulfate (Duchefa), referred to here as YPD<sub>G418r</sub>, or on YPD solid medium containing 100  $\mu$ g/mL hygromycin B (Sigma), referred to here as YPD<sub>HVB</sub>. Gene sequence information was obtained from the *C. neoformans* serotype A genome database (NCBI).

**O-Glycan analysis by HPLC.** For release of the O-glycans, the cell wall mannoproteins (cwMPs) were prepared as described in previous studies (31, 59). Briefly, the completely dried cwMPs (50  $\mu$ g) were resuspended in 100  $\mu$ L of hydrazine monohydrate (Tokyo Chemical Industry), and the mixture was incubated at 60°C for 4 to 6 h. The reactants were dried to remove the hydrazine monohydrate, and the pellets were dissolved in 100  $\mu$ L of saturated NaHCO<sub>3</sub> (Sigma), mixed with 10  $\mu$ L of (CH<sub>3</sub>CO)<sub>2</sub>O, and incubated on ice for 30 min without shaking. The O-glycans were purified by using Dowex 50WX8-400 resins (H<sup>+</sup> form; Sigma), and the isolated O-glycans were labeled with 2-aminobenzoic acid (2-AA; Sigma) and purified using a cyano base cartridge (Bond Elut-CN-E; Agilent) (100 mg). The HPLC analysis of the 2-AA-labeled O-glycan was conducted on a TSKgel Amide-80 column (0.46 by 25 cm, 5  $\mu$ m; Tosoh, Tokyo, Japan) at a flow rate of 1.0 mL/min. 2-AA-Oligosaccharides were detected with a 2475 fluorescence detector (Waters) at excitation and emission wavelengths of 360 and 425 nm, respectively. Data were collected using Empower 2 chromatography data software (Waters).

**In silico bioinformatics analysis to identify cell surface sensor proteins from the *C. neoformans* proteome.** Two candidates of cell wall stress sensors in *C. neoformans* and various cell wall proteins related to the CWI pathway in *S. cerevisiae*, *C. albicans*, and *S. pombe* were analyzed using InterPro (<https://www.ebi.ac.uk/interpro/>), SignalP (<https://services.healthtech.dtu.dk/service.php?SignalP-5.0>), TMHMM (<https://services.healthtech.dtu.dk/service.php?TMHMM-2.0>), YinOYang (<https://services.healthtech.dtu.dk/service.php?YinOYang-1.2>) and NetOGlyc 4.0 (<https://services.healthtech.dtu.dk/service.php?NetOGlyc-4.0>), as follows. First, *C. neoformans* proteins containing a region of 40 amino acids in which the percentage of Ser/Thr was  $\geq$ 40% were identified from the *C. neoformans* proteome, resulting in 958 proteins (12% of the *C. neoformans* proteome). Then, a more restrictive search was carried out for membrane-attached proteins containing a single-pass transmembrane domain in the C-terminal region, narrowing to 80 proteins from the *C. neoformans* database (1% of the *C. neoformans* proteome). The third and fourth search criteria were the absence of a GPI-anchor domain but the presence of a signal peptide at the N-terminal region, respectively. This iterative search resulted in 12 candidate proteins. Additional screening of these 12 proteins was performed with the NetOGlyc server (<https://services.healthtech.dtu.dk/service.php?NetOGlyc-4.0>) to predict O-glycosylation sites, and two putative cell wall sensors of *C. neoformans*, CNAG\_01255 and CNAG\_03328, were finally selected. Multiple sequence alignments and percentage identity were analyzed by the CLUSTALW method of the DNASTAR MegAlign program. A phylogenetic tree based on the sequences of the cell wall stress sensor homologs was constructed using the maximum likelihood tree of the MEGA X software.

**Animal study.** Animal studies were conducted at the Chung-Ang University Animal Experiment Center and were approved by the Ministry of Food and Drug Safety (MFDS; South Korea). The experimenter completed an animal experimental education and followed the guidelines. *C. neoformans* strains (H99, *ltr3Δ*, *cap6Δ*, *ltr3Δ cap6Δ*, and *ltr3Δ cap6Δ::CAP6* strains) were washed with sterile phosphate-buffered saline (PBS) and then resuspended in sterile PBS at a density of  $2 \times 10^6$  cells per mL. Ten mice (6-week-old female A/J Slc mice, 16 to 18 g; Japan SLC) per strain were infected via intranasal instillation of  $10^5$  cells (in 50  $\mu$ L). Following infection, the mice were weighed and monitored once daily and then sacrificed using CO<sub>2</sub> when they lost 30% of the original body weight rapidly. Kaplan-Meier survival curves were generated by using Prism 5.02 (GraphPad Software).

For the fungal burden assay, five mice per strain were infected with *C. neoformans* strains (H99, *ltr3Δ cap6Δ*, and *ltr3Δ cap6Δ::CAP6* strains). The lungs and brains of *C. neoformans*-infected mice ( $n = 5$  for each strain, except  $n = 4$  for WT strain due to death on day 20) were dissected on day 21. Lungs and brains were excised, and half organ portions were analyzed by quantitative culture of CFU. For histopathological analysis, half lung and brain samples were fixed and mucicarmine staining was performed. After slide preparation, each sample was observed using a Zeiss AxioScope (A1) equipped with an AxioCam MRm digital camera.

**In vitro host cell interaction analysis.** To analyze adhesion efficiency of *C. neoformans* cells to epithelial lung cells (A549), A549 cells ( $2 \times 10^5$ ) were seeded into 24-well plates in Dulbecco's modified Eagle's medium (DMEM; Gibco) supplemented with 10% fetal bovine serum (FBS) and cultivated at 37°C in 5% CO<sub>2</sub> for 18 h. Yeast cells ( $2 \times 10^6$ ) were added to each well (*C. neoformans*/A549 ratio, 10:1) and coincubated for 1 h. Then, nonadherent yeast cells were removed by washing with PBS, and the A549 cells were lysed in distilled water. The number of yeast cells was assessed by CFU analysis in three independent experiments. The uptake of *C. neoformans* cells by macrophages was analyzed with the *C. neoformans* cells opsonized with 10  $\mu$ g/mL mouse immunoglobulin G 18B7 antibody (kindly gifted by Arturo Casadevall, Johns Hopkins School of Public Health) at 37°C for 1 h. The macrophage-like J774A.1 cells ( $1 \times 10^5$ ) were seeded into 96-well plates in DMEM supplemented with 10% FBS and cultivated at

37°C in 5% CO<sub>2</sub> for 18 h. Opsonized *C. neoformans* cells ( $1 \times 10^5$ ) were added to activated macrophages (*C. neoformans*/J774A.1 ratio, 1:1) and incubated with serum-free DMEM. After 1 h of coinubation, non-phagocytized yeast cells were removed by washing and the macrophages were lysed in distilled water. The number of *C. neoformans* cells phagocytized by macrophages was assessed by CFU analysis in three independent experiments. To analyze the fungal cell survival in macrophages (J774A.1), after 1 h of coinubation, each well was washed to remove extracellular yeast cells. Then, 100  $\mu$ L of macrophage medium was added to each well and the *C. neoformans*-infected macrophages were incubated for 24 h. Then, macrophages were lysed in distilled water by vigorous pipetting, and the fungal cells were collected, serially diluted, and plated onto a YPD plate to assess the number of viable *C. neoformans* cells.

**Analysis of host immune response by cytokine and LDH analysis.** For analysis of secreted cytokines, activated BMDCs were prepared as previously described (39) with slight modification. The BMDCs ( $1 \times 10^5$  cells/well) were inoculated into 96-well plates (in RPMI medium plus 10% heat-inactivated FBS) and incubated at 37°C in 5% CO<sub>2</sub> for 1 h. The BMDCs were then incubated with cryptococcal cells ( $1 \times 10^6$  cells/well) for 12 h, and the supernatants were collected and centrifuged at  $17,000 \times g$  for 5 min. Released levels of TNF- $\alpha$  and IL-6 were analyzed by enzyme-linked immunosorbent assay using mouse TNF- $\alpha$  ELISA Max set deluxe kits and mouse IL-6 ELISA Max set deluxe kits (BioLegend), according to the manufacturer's instructions.

For analysis of host cell lysis, *C. neoformans* cells were washed twice with PBS, counted, and added to BMDCs at a concentration of  $2 \times 10^6$  cells/well. After incubation for the indicated time (3 h, 6 h, or 16 h), supernatants were collected and centrifuged at  $17,000 \times g$  for 5 min. Levels of released IL-1 $\beta$  were analyzed by enzyme-linked immunosorbent assay (ELISA) using mouse IL-1 $\beta$  ELISA Max set deluxe kits (BioLegend), according to the manufacturer's instructions. Levels of LDH enzyme released into the cell culture supernatant were measured as a colorimetric change using an LDH cytotoxicity detection kit (Pierce) according to the manufacturer's protocol. The plate was read at 490 nm using a microplate reader after 30 min of incubation at room temperature. The absorbance was measured, and percent cytotoxicity was calculated for the samples.

**hCMEC/D3 cell adhesion and BBB transmigration assays.** *In vitro* BBB adhesion and transmigration assays were performed as previously described (60). Briefly, a human brain microvascular endothelial cell (hBMEC) line (hCMEC/D3 cell line; Merck) was cultured at 37°C with 5% CO<sub>2</sub> in EGM-2 medium (Lonza). For the BBB adhesion assay,  $5 \times 10^4$  hCMEC/D3 cells in EGM-2 medium were seeded on collagen-coated 12-well plates (BD Falcon) and cultured until the monolayer became confluent. A day before *C. neoformans* inoculation, the EGM-2 medium (2.5% human serum) was replaced with EGM-2 medium (1.25% human serum), and integrity of tight junction formation was measured as transendothelial electrical resistance (TEER) using an epithelial volt per ohm meter (EVOM<sup>2</sup> device; World Precision Instruments). hCMEC/D3 cells were coinubated with  $5 \times 10^5$  fungal cells for 24 h, and then the endothelial barrier was washed to remove nonadherent cells and lysed with water to determine the number of cells that adhere to the barrier.

For the BBB crossing assay, hCMEC/D3 cells were seeded in a transwell chamber and cultured as described as above. *C. neoformans* cells were inoculated onto the top of the porous membranes. After 24 h of incubation, the medium in the bottom chambers was collected and the number of yeast cells passing through the porous membrane was measured by counting the CFU. The BBB adhesion or migration ratio was calculated by dividing the output CFU of each tested strain by that of the WT.

**Ergosterol staining analysis.** For ergosterol staining, *C. neoformans* cells at an OD<sub>600</sub> of 0.3 were cultivated in 25 mL YPD at 30°C for 6 h. The cell pellets were washed with PBS and fixed with 4% paraformaldehyde (PFA) solution for 20 min on an 18-rpm rotator. After washing with PBS, the cells were stained with 10  $\mu$ g/mL filipin III (Cayman Chemical, Ann Arbor, MI) in the dark for 5 min on an 18-rpm rotator. After washing with PBS, cell pellets were resuspended in 500  $\mu$ L PBS and observed immediately. Cells were visualized with an Eclipse Ti-E fluorescence microscope (Nikon) equipped with a Nikon DS-Qi2 camera and a Plan Apo VC 100 $\times$  oil differential interference contrast (DIC) N2 (numerical aperture, 1.4) lens using an excitation of 360 nm and an emission of 480 nm. Images were processed based on the NIS-Elements microscope imaging software (Nikon).

**Ergosterol extraction and analysis.** Total intracellular sterols were extracted using KOH-heptane (53). Briefly, *C. neoformans* cells, cultivated in YPD liquid medium at 30°C for 48 h, were washed three times with PBS. Subsequently, cell cultures were centrifuged and resuspended in 1 mL KOH-H<sub>2</sub>O-ethanol (EtOH) per 0.1 g wet weight of cell pellet. After incubation 1 h at 85°C, 500  $\mu$ L heptane was added to the mixture and stirred using a Precellys 24 tissue homogenizer (Bertin Technologies) at 6,500 rpm for 30 s. The mixtures were centrifuged at 13,000 rpm for 15 min, and the supernatants were collected and freeze-dried overnight.

For ergosterol analysis, the total intracellular sterol extract was dissolved in 250  $\mu$ L of acetone. After filtration, the samples were subjected to HPLC analysis using a COSMOSIL 5C18-PAQ packed column (120  $\text{\AA}$ , 5  $\mu$ m, 4.6 mm inner diameter by 250 mm) at a flow rate of 1.0 mL/min. Ergosterol was detected with a Waters 2487 absorbance detector at wavelengths of 203 nm. Data were collected using Empower 2 chromatography data software (Waters).

**Data availability.** Raw RNA sequencing data have been submitted to the NCBI GEO database under accession no. [GSE198875](https://www.ncbi.nlm.nih.gov/geo/query/acc.cgi?acc=GSE198875).

## SUPPLEMENTAL MATERIAL

Supplemental material is available online only.

**TEXT S1**, DOCX file, 0.05 MB.

**FIG S1**, TIF file, 1.6 MB.

**FIG S2**, TIF file, 2.9 MB.

**FIG S3**, TIF file, 2 MB.

**FIG S4**, TIF file, 1 MB.

**FIG S5**, TIF file, 1.6 MB.

**FIG S6**, TIF file, 1.2 MB.

**FIG S7**, TIF file, 1.6 MB.

**FIG S8**, TIF file, 1.4 MB.

**TABLE S1**, DOCX file, 0.05 MB.

## ACKNOWLEDGMENTS

This research was supported by the National Research Foundation of Korea (grant no. NRF2022R1A2C1012699 and NRF2018R1A5A1025077). This work was also partly supported by the Chung-Ang University Graduate Research Scholarship 2021.

## REFERENCES

- Lehle L, Strahl S, Tanner W. 2006. Protein glycosylation, conserved from yeast to man: a model organism helps elucidate congenital human diseases. *Angew Chem Int Ed Engl* 45:6802–6818. <https://doi.org/10.1002/anie.200601645>.
- Lommel M, Strahl S. 2009. Protein O-mannosylation: conserved from bacteria to humans. *Glycobiology* 19:816–828. <https://doi.org/10.1093/glycob/cwp066>.
- Gentzsch M, Tanner W. 1997. Protein-O-glycosylation in yeast: protein-specific mannosyltransferases. *Glycobiology* 7:481–486. <https://doi.org/10.1093/glycob/7.4.481>.
- Strahl-Bolsinger S, Gentzsch M, Tanner W. 1999. Protein O-mannosylation. *Biochim Biophys Acta* 1426:297–307. [https://doi.org/10.1016/S0304-4165\(98\)00131-7](https://doi.org/10.1016/S0304-4165(98)00131-7).
- Deshpande N, Wilkins MR, Packer N, Nevalainen H. 2008. Protein glycosylation pathways in filamentous fungi. *Glycobiology* 18:626–637. <https://doi.org/10.1093/glycob/cwn044>.
- Gemmill TR, Trimble RB. 1999. Overview of N- and O-linked oligosaccharide structures found in various yeast species. *Biochim Biophys Acta* 1426:227–237. [https://doi.org/10.1016/S0304-4165\(98\)00126-3](https://doi.org/10.1016/S0304-4165(98)00126-3).
- Goto M. 2007. Protein O-glycosylation in fungi: diverse structures and multiple functions. *Biosci Biotechnol Biochem* 71:1415–1427. <https://doi.org/10.1271/bbb.70080>.
- Mille C, Bobrowicz P, Trinel PA, Li H, Maes E, Guerardel Y, Fradin C, Martínez-Esparza M, Davidson RC, Janbon G, Poulain D, Wildt S. 2008. Identification of a new family of genes involved in beta-1,2-mannosylation of glycans in *Pichia pastoris* and *Candida albicans*. *J Biol Chem* 283:9724–9736. <https://doi.org/10.1074/jbc.M708825200>.
- Darula Z, Medzihradsky KF. 2018. Analysis of mammalian O-glycopeptides—we have made a good start, but there is a long way to go. *Mol Cell Proteomics* 17:2–17. <https://doi.org/10.1074/mcp.MR117.000126>.
- Olson GM, Fox DS, Wang P, Alspaugh JA, Buchanan KL. 2007. Role of protein O-mannosyltransferase Pmt4 in the morphogenesis and virulence of *Cryptococcus neoformans*. *Eukaryot Cell* 6:222–234. <https://doi.org/10.1128/EC.00182-06>.
- Proszynski TJ, Simons K, Bagnat M. 2004. O-Glycosylation as a sorting determinant for cell surface delivery in yeast. *Mol Biol Cell* 15:1533–1543. <https://doi.org/10.1091/mbc.e03-07-0511>.
- Weber Y, Prill SK, Ernst JF. 2004. Pmt-mediated O-mannosylation stabilizes an essential component of the secretory apparatus, Sec20p, in *Candida albicans*. *Eukaryot Cell* 3:1164–1168. <https://doi.org/10.1128/EC.3.5.1164-1168.2004>.
- Lengeler KB, Tielker D, Ernst JF. 2008. Protein-O-mannosyltransferases in virulence and development. *Cell Mol Life Sci* 65:528–544. <https://doi.org/10.1007/s00018-007-7409-z>.
- Prill SK, Klinkert B, Timpel C, Gale CA, Schröppel K, Ernst JF. 2005. PMT family of *Candida albicans*: five protein mannosyltransferase isoforms affect growth, morphogenesis and antifungal resistance. *Mol Microbiol* 55:546–560. <https://doi.org/10.1111/j.1365-2958.2004.04401.x>.
- Munro CA, Bates S, Buurman ET, Hughes HB, Maccallum DM, Bertram G, Atrih A, Ferguson MA, Bain JM, Brand A, Hamilton S, Westwater C, Thomson LM, Brown AJ, Odds FC, Gow NA. 2005. Mnt1p and Mnt2p of *Candida albicans* are partially redundant alpha-1,2-mannosyltransferases that participate in O-linked mannosylation and are required for adhesion and virulence. *J Biol Chem* 280:1051–1060. <https://doi.org/10.1074/jbc.M411413200>.
- Wagener J, Echtenacher B, Rohde M, Kotz A, Krappmann S, Heesemann J, Ebel F. 2008. The putative alpha-1,2-mannosyltransferase AfMnt1 of the opportunistic fungal pathogen *Aspergillus fumigatus* is required for cell wall stability and full virulence. *Eukaryot Cell* 7:1661–1673. <https://doi.org/10.1128/EC.00221-08>.
- Garfoot AL, Goughenour KD, Wüthrich M, Rajaram MVS, Schlesinger LS, Klein BS, Rappleye CA. 2018. O-Mannosylation of proteins enables Histoplasma yeast survival at mammalian body temperatures. *mBio* 9:e02121-17. <https://doi.org/10.1128/mBio.02121-17>.
- Pan Y, Pan R, Tan L, Zhang Z, Guo M. 2019. Pleiotropic roles of O-mannosyltransferase MoPmt4 in development and pathogenicity of *Magnaporthe oryzae*. *Curr Genet* 65:223–239. <https://doi.org/10.1007/s00294-018-0864-2>.
- Xu Y, Zhou H, Zhao G, Yang J, Luo Y, Sun S, Wang Z, Li S, Jin C. 2020. Genetical and O-glycoproteomic analyses reveal the roles of three protein O-mannosyltransferases in phytopathogen *Fusarium oxysporum* f.sp. *cucumerinum*. *Fungal Genet Biol* 134:103285. <https://doi.org/10.1016/j.fgb.2019.103285>.
- Gómez-Gaviria M, Vargas-Macias AP, García-Carnero LC, Martínez-Duncker I, Mora-Montes HM. 2021. Role of protein glycosylation in interactions of medically relevant fungi with the host. *J Fungi (Basel)* 7:875. <https://doi.org/10.3390/jof7100875>.
- Murciano C, Moyes DL, Rungrall M, Islam A, Mille C, Fradin C, Poulain D, Gow NA, Naglik JR. 2011. *Candida albicans* cell wall glycosylation may be indirectly required for activation of epithelial cell proinflammatory responses. *Infect Immun* 79:4902–4911. <https://doi.org/10.1128/IAI.05591-11>.
- O'Meara TR, Cowen LE. 2018. Insights into the host-pathogen interaction: *C. albicans* manipulation of macrophage pyroptosis. *Microb Cell* 5:566–568. <https://doi.org/10.15698/mic2018.12.662>.
- O'Meara TR, Veri AO, Ketela T, Jiang B, Roemer T, Cowen LE. 2015. Global analysis of fungal morphology exposes mechanisms of host cell escape. *Nat Commun* 6:6741. <https://doi.org/10.1038/ncomms7741>.
- Koselny K, Mutlu N, Minard AY, Kumar A, Krysan DJ, Wellington M. 2018. A genome-wide screen of deletion mutants in the filamentous *Saccharomyces cerevisiae* background identifies ergosterol as a direct trigger of macrophage pyroptosis. *mBio* 9:e01204-18. <https://doi.org/10.1128/mBio.01204-18>.
- Perfect JR, Casadevall A. 2002. Cryptococcosis. *Infect Dis Clin North Am* 16:837–874. [https://doi.org/10.1016/S0891-5520\(02\)00036-3](https://doi.org/10.1016/S0891-5520(02)00036-3).
- Maruvada R, Zhu L, Pearce D, Zheng Y, Perfect J, Kwon-Chung KJ, Kim KS. 2012. *Cryptococcus neoformans* phospholipase B1 activates host cell Rac1 for traversal across the blood-brain barrier. *Cell Microbiol* 14:1544–1553. <https://doi.org/10.1111/j.1462-5822.2012.01819.x>.
- Wozniak KL, Levitz SM. 2009. Isolation and purification of antigenic components of *Cryptococcus*. *Methods Mol Biol* 470:71–83. [https://doi.org/10.1007/978-1-59745-204-5\\_7](https://doi.org/10.1007/978-1-59745-204-5_7).
- Mansour MK, Latz E, Levitz SM. 2006. *Cryptococcus neoformans* glycoantigens are captured by multiple lectin receptors and presented by dendritic cells. *J Immunol* 176:3053–3061. <https://doi.org/10.4049/jimmunol.176.5.3053>.

29. Willger SD, Ernst JF, Alspaugh JA, Lengeler KB. 2009. Characterization of the PMT gene family in *Cryptococcus neoformans*. *PLoS One* 4:e6321. <https://doi.org/10.1371/journal.pone.0006321>.
30. Reilly MC, Aoki K, Wang ZA, Skowrya ML, Williams M, Tiemeyer M, Doering TL. 2011. A xylosylphosphotransferase of *Cryptococcus neoformans* acts in protein O-glycan synthesis. *J Biol Chem* 286:26888–26899. <https://doi.org/10.1074/jbc.M111.262162>.
31. Lee DJ, Bahn YS, Kim HJ, Chung SY, Kang HA. 2015. Unraveling the novel structure and biosynthetic pathway of O-linked glycans in the Golgi apparatus of the human pathogenic yeast *Cryptococcus neoformans*. *J Biol Chem* 290:1861–1873. <https://doi.org/10.1074/jbc.M114.607705>.
32. Cherniak R, Valafar H, Morris LC, Valafar F. 1998. *Cryptococcus neoformans* chemotyping by quantitative analysis of 1H nuclear magnetic resonance spectra of glucuronoxylomannans with a computer-simulated artificial neural network. *Clin Diagn Lab Immunol* 5:146–159. <https://doi.org/10.1128/CDLI.5.2.146-159.1998>.
33. Klutts JS, Levery SB, Doering TL. 2007. A beta-1,2-xylosyltransferase from *Cryptococcus neoformans* defines a new family of glycosyltransferases. *J Biol Chem* 282:17890–17899. <https://doi.org/10.1074/jbc.M701941200>.
34. Park JN, Lee DJ, Kwon O, Oh DB, Bahn YS, Kang HA. 2012. Unraveling unique structure and biosynthesis pathway of N-linked glycans in human fungal pathogen *Cryptococcus neoformans* by glycomics analysis. *J Biol Chem* 287:19501–19515. <https://doi.org/10.1074/jbc.M112.354209>.
35. Sommer U, Liu H, Doering TL. 2003. An alpha-1,3-mannosyltransferase of *Cryptococcus neoformans*. *J Biol Chem* 278:47724–47730. <https://doi.org/10.1074/jbc.M307223200>.
36. O'Meara TR, Alspaugh JA. 2012. The *Cryptococcus neoformans* capsule: a sword and a shield. *Clin Microbiol Rev* 25:387–408. <https://doi.org/10.1128/CMR.00001-12>.
37. Moyrand F, Fontaine T, Janbon G. 2007. Systematic capsule gene disruption reveals the central role of galactose metabolism on *Cryptococcus neoformans* virulence. *Mol Microbiol* 64:771–781. <https://doi.org/10.1111/j.1365-2958.2007.05695.x>.
38. Huang C, Nong SH, Mansour MK, Specht CA, Levitz SM. 2002. Purification and characterization of a second immunoreactive mannoprotein from *Cryptococcus neoformans* that stimulates T-cell responses. *Infect Immun* 70:5485–5493. <https://doi.org/10.1128/IAI.70.10.5485-5493.2002>.
39. Thak EJ, Lee SB, Xu-Vanpala S, Lee DJ, Chung SY, Bahn YS, Oh DB, Shinohara ML, Kang HA. 2020. Core N-glycan structures are critical for the pathogenicity of *Cryptococcus neoformans* by modulating host cell death. *mBio* 11:e00711-20. <https://doi.org/10.1128/mBio.00711-20>.
40. Kock C, Dufrene YF, Heinisch JJ. 2015. Up against the wall: is yeast cell wall integrity ensured by mechanosensing in plasma membrane microdomains? *Appl Environ Microbiol* 81:806–811. <https://doi.org/10.1128/AEM.03273-14>.
41. Cheon SA, Jung KW, Chen YL, Heitman J, Bahn YS, Kang HA. 2011. Unique evolution of the UPR pathway with a novel bZIP transcription factor, Hx11, for controlling pathogenicity of *Cryptococcus neoformans*. *PLoS Pathog* 7:e1002177. <https://doi.org/10.1371/journal.ppat.1002177>.
42. Kim SY, Ko YJ, Jung KW, Strain A, Nielsen K, Bahn YS. 2011. Hrk1 plays both Hog1-dependent and -independent roles in controlling stress response and antifungal drug resistance in *Cryptococcus neoformans*. *PLoS One* 6:e18769. <https://doi.org/10.1371/journal.pone.0018769>.
43. So YS, Jang J, Park G, Xu J, Olszewski MA, Bahn YS. 2018. Sho1 and Msb2 play complementary but distinct roles in stress responses, sexual differentiation, and pathogenicity of *Cryptococcus neoformans*. *Front Microbiol* 9:2958. <https://doi.org/10.3389/fmicb.2018.02958>.
44. Bahn YS, Kojima K, Cox GM, Heitman J. 2006. A unique fungal two-component system regulates stress responses, drug sensitivity, sexual development, and virulence of *Cryptococcus neoformans*. *Mol Biol Cell* 17:3122–3135. <https://doi.org/10.1091/mbc.e06-02-0113>.
45. Bonilla M, Cunningham KW. 2003. Mitogen-activated protein kinase stimulation of Ca(2+) signaling is required for survival of endoplasmic reticulum stress in yeast. *Mol Biol Cell* 14:4296–4305. <https://doi.org/10.1091/mbc.e03-02-0113>.
46. Kraus PR, Fox DS, Cox GM, Heitman J. 2003. The *Cryptococcus neoformans* MAP kinase Mpk1 regulates cell integrity in response to antifungal drugs and loss of calcineurin function. *Mol Microbiol* 48:1377–1387. <https://doi.org/10.1046/j.1365-2958.2003.03508.x>.
47. Jin JH, Lee KT, Hong J, Lee D, Jang EH, Kim JY, Lee Y, Lee SH, So YS, Jung KW, Lee DG, Jeong E, Lee M, Jang YB, Choi Y, Lee MH, Kim JS, Yu SR, Choi JT, La JW, Choi H, Kim SW, Seo KJ, Lee Y, Thak EJ, Choi J, Averette AF, Lee YH, Heitman J, Kang HA, Cheong E, Bahn YS. 2020. Genome-wide functional analysis of phosphatases in the pathogenic fungus *Cryptococcus neoformans*. *Nat Commun* 11:4212. <https://doi.org/10.1038/s41467-020-18028-0>.
48. Na Pombejra S, Salemi M, Phinney BS, Gelli A. 2017. The metalloprotease, Mpr1, engages annexinA2 to promote the transcytosis of fungal cells across the blood-brain barrier. *Front Cell Infect Microbiol* 7:296. <https://doi.org/10.3389/fcimb.2017.00296>.
49. Vu K, Tham R, Uhrig JP, Thompson GR, 3rd, Na Pombejra S, Jamklang M, Bautos JM, Gelli A. 2014. Invasion of the central nervous system by *Cryptococcus neoformans* requires a secreted fungal metalloprotease. *mBio* 5:e01101-14. <https://doi.org/10.1128/mBio.01101-14>.
50. Wozniak KL, Vyas JM, Levitz SM. 2006. *In vivo* role of dendritic cells in a murine model of pulmonary cryptococcosis. *Infect Immun* 74:3817–3824. <https://doi.org/10.1128/IAI.00317-06>.
51. Rodrigues ML. 2018. The multifunctional fungal ergosterol. *mBio* 9:e01755-18. <https://doi.org/10.1128/mBio.01755-18>.
52. Baumann NA, Sullivan DP, Ohvo-Rekila H, Simonot C, Pottekat A, Klaassen Z, Beh CT, Menon AK. 2005. Transport of newly synthesized sterol to the sterol enriched plasma membrane occurs via nonvesicular equilibration. *Biochemistry* 44:5816–5826. <https://doi.org/10.1021/bi048296z>.
53. Arthington-Skaggs BA, Jradi H, Desai T, Morrison CJ. 1999. Quantitation of ergosterol content: novel method for determination of fluconazole susceptibility of *Candida albicans*. *J Clin Microbiol* 37:3332–3337. <https://doi.org/10.1128/JCM.37.10.3332-3337.1999>.
54. Dichtl K, Samantaray S, Wagener J. 2016. Cell wall integrity signalling in human pathogenic fungi. *Cell Microbiol* 18:1228–1238. <https://doi.org/10.1111/cmi.12612>.
55. Yabuki Y, Ikeda A, Araki M, Kajiwara K, Mizuta K, Funato K. 2019. Sphingolipid/Pkh1/2-TORC1/Sch9 signaling regulates ribosome biogenesis in tunicamycin-induced stress response in yeast. *Genetics* 212:175–186. <https://doi.org/10.1534/genetics.118.301874>.
56. Lippman SI, Broach JR. 2009. Protein kinase A and TORC1 activate genes for ribosomal biogenesis by inactivating repressors encoded by Dot6 and its homolog Tod6. *Proc Natl Acad Sci U S A* 106:19928–19933. <https://doi.org/10.1073/pnas.0907027106>.
57. Sánchez-Adriá IE, Sanmartín G, Prieto JA, Estruch F, Rande-Gil F. 2022. Slt2 is required to activate ER-stress-protective mechanisms through TORC1 inhibition and hexosamine pathway activation. *J Fungi (Basel)* 8:92. <https://doi.org/10.3390/jof8020092>.
58. Petkova MI, Pujol-Carrion N, de la Torre-Ruiz MA. 2012. Mtl1 O-mannosylation mediated by both Pmt1 and Pmt2 is important for cell survival under oxidative conditions and TOR blockade. *Fungal Genet Biol* 49:903–914. <https://doi.org/10.1016/j.fgb.2012.08.005>.
59. Thak EJ, Kim J, Lee DJ, Kim JY, Kang HA. 2018. Structural analysis of N-O-glycans assembled on proteins in yeasts. *J Microbiol* 56:11–23. <https://doi.org/10.1007/s12275-018-7468-x>.
60. Lee KT, Hong J, Lee DG, Lee M, Cha S, Lim YG, Jung KW, Hwangbo A, Lee Y, Yu SJ, Chen YL, Lee JS, Cheong E, Bahn YS. 2020. Fungal kinases and transcription factors regulating brain infection in *Cryptococcus neoformans*. *Nat Commun* 11:1521. <https://doi.org/10.1038/s41467-020-15329-2>.